Mon. Not. R. Astron. Soc. **389,** 585–607 (2008) doi:10.1111/j.1365-2966.2008.13573.x

M dwarfs: effective temperatures, radii and metallicities

Luca Casagrande,[1]★ Chris Flynn[1] and Michael Bessell[2]

[1]*Tuorla Observatory, Department of Physics and Astronomy, University of Turku, Väisäläntie 20, FI-21500 Piikkiö, Finland*
[2]*Research School of Astronomy & Astrophysics, Australian National University, Cotter Road, Weston, ACT 2611, Australia*

Accepted 2008 June 10. Received 2008 June 10; in original form 2008 January 29

ABSTRACT

We empirically determine effective temperatures and bolometric luminosities for a large sample of nearby M dwarfs, for which high accuracy optical and infrared photometry is available. We introduce a new technique which exploits the flux ratio in different bands as a proxy of both effective temperature and metallicity. Our temperature scale for late-type dwarfs extends well below 3000 K (almost to the brown dwarf limit) and is supported by interferometric angular diameter measurements above 3000 K. Our metallicities are in excellent agreement (usually within 0.2 dex) with recent determinations via independent techniques. A subsample of cool M dwarfs with metallicity estimates based on hotter *Hipparcos* common proper motion companions indicates our metallicities are also reliable below 3000 K, a temperature range unexplored until now. The high quality of our data allows us to identify a striking feature in the bolometric luminosity versus temperature plane, around the transition from K to M dwarfs. We have compared our sample of stars with theoretical models and conclude that this transition is due to an increase in the radii of the M dwarfs, a feature which is not reproduced by theoretical models.

Key words: stars: abundances – stars: atmospheres – stars: fundamental parameters – Hertzsprung–Russell (HR) diagram – stars: low-mass, brown dwarf – infrared: stars.

1 INTRODUCTION

Low-mass dwarfs are the dominant stellar component of the Galaxy and have been employed in a variety of Galactic studies: tracing Galactic disc kinematics (e.g. Hawley, Gizis & Reid 1996; Gizis, Reid & Hawley 2002; Bochanski et al. 2005, 2007), studying the stellar age–velocity relations (West et al. 2006), investigating Galactic structure (e.g. Reid et al. 1997; Kerber, Javiel & Santiago 2001; Pirzkal et al. 2005) and the Galaxy's mass and luminosity (e.g. Hawkins & Bessell 1988; Kirkpatrick et al. 1994; Gould, Bahcall & Flynn 1997; Gould, Flynn & Bahcall 1998; Zheng et al. 2001, 2004). An increasing number of M dwarfs are now known to host exoplanets (e.g. Delfosse et al. 1998; Butler et al. 2004; Bonfils et al. 2007; Udry et al. 2007). The determination of accurate fundamental parameters for M dwarfs has therefore relevant implications for both stellar and Galactic astronomy.

Observationally, the spectra of these stars are marked by the presence of strong molecular absorption features, in either optical (e.g. TiO and VO) or infrared (IR) regions (e.g. H_2O and CO). Molecular lines blend with all other lines and create a pseudo-continuum, rendering all spectral analysis difficult (e.g. Gustafsson 1989). However, recent advances in model atmospheres of low-mass dwarf stars (Hauschildt et al. 2003; Brott & Hauschildt 2005) have boosted the number of studies deriving accurate metallicities for M dwarfs (Woolf & Wallerstein 2005, 2006; Bean et al. 2006a,b). Modelling the internal structure, atmospheric properties and magnetic activity of M dwarfs (e.g. Burrows et al. 1993; Allard et al. 1997; Baraffe et al. 1998; Hauschildt, Allard & Baron 1999a; Allred et al. 2006; Reiners & Basri 2007) also presents ongoing theoretical challenges. For a small number of nearby M dwarfs, interferometry is currently providing direct angular diameter measurements (Lane, Boden & Kulkarni 2001; Ségransan et al. 2003; Berger et al. 2006) which confirm a large discrepancy between the predicted and observed radii, as has been noted in eclipsing binaries with M-type components (see Ribas 2006, for a review).

In this paper, we empirically determine the effective temperatures and the bolometric luminosities for more than 340 M dwarfs. This work is an extension of our previous study on G and K dwarfs, to which we applied the infrared flux method (IRFM; Casagrande, Portinari & Flynn 2006). The effective temperature and the bolometric luminosity scales we derive are accurate at a level of a few per cent and are supported by interferometric angular diameters above ∼3000 K.

We find in this study that below about 4000 K the monochromatic to bolometric flux ratio in different bands is a proxy of both effective temperature and metallicity. By exploiting this feature, we are able to derive not only $T_{\rm eff}$ but also the metallicities of our M dwarfs, which are found to be in very good agreement (usually within 0.2–0.3 dex) with those inferred using the Bonfils et al. (2005) calibration or directly measured from Woolf & Wallerstein (2005, 2006). The technique we propose also looks promising

★E-mail: luccas@utu.fi

© 2008 The Authors. Journal compilation © 2008 RAS

Downloaded from http://mnras.oxfordjournals.org/ by guest on January 20, 2015

for stars much cooler than those explored in the aforementioned studies.

We find considerable structure in the temperature–luminosity plane, especially around the transition between K and M dwarfs. Our study circumstantially confirms previous works which indicate that the radii of M dwarfs are larger by about 15 per cent than model predictions. We also find strong evidence that this discrepancy, clearly observed in M dwarfs in eclipsing binary systems, is also present in nearby disc M dwarfs.

The paper is organized as follows. In Section 2 we describe our sample of M dwarfs and in Section 3 we compare it with the Phoenix model atmosphere in the two-colour plane. We then review the IRFM and present our new technique for estimating effective temperatures and metallicities below 4000 K in Section 4. Our proposed metallicity, bolometric luminosity and effective temperature scales along with the comparison with other empirical determinations are discussed in Sections 5, 6 and 7, respectively. In Section 8 we analyse the stars with good *Hipparcos* parallaxes in the HR diagram. We find a strong feature which marks the transition from K to M dwarfs and which is due to an increase in the observed stellar radii. We briefly discuss possible reasons, including the effect of magnetic fields and molecular opacity. We finally conclude in Section 9.

2 THE SAMPLE

Our basic sample consists of 343 nearby M dwarfs with high-quality optical and IR photometry. We describe the sample selection in this section.

2.1 Johnson–Cousins photometry

In recent years major efforts have been devoted to obtaining high accuracy Johnson–Cousins photometry for cool stars (Kilkenny et al. 1998, 2007; Koen et al. 2002). One third of our sample is built from the extensive work of Koen et al. (2002) who presented homogeneous and standardized $UBV(RI)_{\rm C}$ photometry for more than 500 M stars, half of which are main-sequence dwarfs. Variability has a very high incidence among cool stars; however, the existence of $\sim$100 or more *Hipparcos* measurements per star spread over several years, together with the excellent temporal stability of the magnitude scale, permits the detection of variability at the level of few hundredths of a magnitude. The red standards provided by Koen et al. (2002) are all non-variables in this sense (i.e. the *Hipparcos* variability flag is not set); Koen et al. (2002) also provide the SIMBAD and CCDM (Dommanget & Nys 1994) classification for variability and double/multiple stars. We have discarded all star having those labels, for a total final sample 128 M dwarfs. Besides Johnson–Cousins photometry accurate to 0.01 mag or better, all these stars have *Hipparcos* parallaxes better than 15 per cent and are all closer than 60 pc.

Another accurate source of Johnson–Cousins photometry for M dwarfs is Reid, Kilkenny & Cruz (2002) and Reid et al. (2003, 2004). Altogether, they provided new $V(RI)_{\rm C}$ (and B for the brightest sources) measurements for more than 370 NLTT (New Luyten Two Tenths) stars. We have used the SIMBAD classification plus the essential notes as given in the aforementioned papers to remove double, variables, flares, possible misclassification and stars with nearby companions (or background stars) that could affect the photometric measurements. The photometry is accurate and consistent with the standard photometric system to better than 1 per cent (Reid et al. 2002) and with a typical uncertainty less than 2 per cent even for single night observations (Reid et al. 2003, 2004). Furthermore, all observations are done with the same instrument and reduced using identical methods, similar to those described in Kilkenny et al. (1998) and Koen et al. (2002). Reid et al. (2002, 2003, 2004) also provide photometric distances for all the stars: although such estimates do not provide definitive distance measurements, we have used them to ensure that all the stars chosen are closer than 50 pc and their absolute magnitudes are consistent with those expected from dwarf stars. Altogether, we have retained 94 stars with $BV(RI)_{\rm C}$ and 157 stars with $V(RI)_{\rm C}$ photometry.

We also took a few very red dwarfs from Henry et al. (2004) who measured $V(RI)_{\rm C}$ colours using standards from Graham (1982), Bessell (1990a) and Landolt (1992). These stars are also generally fainter and the accuracy is somewhat lower, with a typical uncertainty of $\pm$0.03 mag in each band (Henry et al. 2004). We have selected 11 such stars, all closer than 40 pc. Finally, another source of $V(RI)_{\rm C}$ photometry for very red stars is from Bessell (1991), from which we took five stars. For the stars in Bessell (1991) and Henry et al. (2004) we have used the SIMBAD classification to avoid flares or variables, although in this case the most affected bands would be the blue ones (U and B) which we do not have for these stars.

2.2 Near-infrared photometry

All the stars presented in Section 2.1 have $JHK_{\rm S}$ photometry from Two Micron All Sky Survey (2MASS). In what follows we will use only stars with total photometric errors (as given from 2MASS) smaller than 0.10 mag (i.e. 'j_'+'h_'+'k_msigcom' $<$0.10), thus reducing our final sample to 343 stars. The typical errors in J and $K_{\rm S}$ are around 0.023 mag, whereas a slightly larger uncertainty (0.032 mag) affects H-band photometry.

For most of the Koen et al. (2002) stars, excellent South African Astronomical Observatory (SAAO) *JHK* photometry is also available (Kilkenny et al. 2007): this additional photometry is very valuable to check the accuracy of the 2MASS zero-points and the dependence of the proposed temperature scale on the adopted absolute calibration. As we show in Appendix B, the SAAO IR photometry confirms the adopted 2MASS zero-points and absolute calibration.

2.3 Metallicities

Measuring metallicities for M dwarfs is still challenging. With decreasing temperature, the spectra show increasingly abundant diatomic and triatomic molecules. The molecular bands complicate the calculation of stellar model atmospheres and cause line blends, making it difficult to estimate the true continuum and to measure atomic line strengths over large regions of the visible spectra.

Major advances in the field have been recently obtained using high-resolution spectra to measure equivalent widths of atomic lines in regions not dominated by molecular bands (Woolf & Wallerstein 2005, 2006). Bonfils et al. (2005) have measured the metallicity in 20 binary systems, having an M dwarf secondary and a warmer primary (for which a metallicity is much more readily obtained). They combined their results with the abundances measured from Woolf & Wallerstein (2005) to calibrate an absolute $K_{\rm S}$-band luminosity versus colour relation [$M_{K_{\rm S}}$ and $(V-K_{\rm S})$] as a function of metallicity. This results in a metallicity relation for M dwarfs, but since it depends on absolute magnitude, we apply it only to those of our stars with accurate parallaxes available from *Hipparcos*. Altogether in our sample there are 118 stars with accurate 2MASS photometry (see Section 2.2), *Hipparcos* parallaxes better then 15 per cent and

Downloaded from http://mnras.oxfordjournals.org/ by guest on January 20, 2015

within the range of applicability of the Bonfils et al. (2005) calibration. The formal accuracy of the relation is ±0.2 dex; however, the uncertainty in parallaxes introduces an additional error that in the worst case can be of the same magnitude. Therefore, we expect these metallicities to be accurate to 0.2–0.3 dex.

In Section 4 we will use these metallicities to calibrate our method to estimate [M/H] for the rest of the M dwarfs.[1]

3 THE PHOENIX MODEL ATMOSPHERES

We apply an extension of the IRFM we developed for G and K dwarfs (Casagrande et al. 2006) to M dwarfs. While most of the bolometric flux of the stars is emitted in the optical and IR and is covered by our observations, as in the earlier work, we use model atmospheres to estimate the small part (typically less than 20 per cent) of the flux which is outside our observational bands.

Pioneering work on M dwarfs model atmospheres trace back to Auman (1969) and Tsuji (1969). The inclusion of sophisticated physics became available with the work of Mould (1975, 1976) and has steadily continued with Allard (1990), Kui (1991), Brett & Plez (1993), Allard & Hauschildt (1995), Brett (1995a,b), Tsuji, Ohnaka & Aoki (1996) and Hauschildt et al. (1999b).

We use the most recent grid of model atmosphere publicly available at the Phoenix project's website.[2] The models cover a range of parameters far wider than that needed for the present work: $2000 \leq T_{\rm eff} \leq 10\,000$ K, $-0.5 \leq \log(g) \leq 5.5$ and $-4.0 \leq$ [M/H] $\leq +0.5$. Below 7000 K the grid is given in steps of 100 K in effective temperature and 0.5 dex in metallicity. The molecular line lists include about 700 million molecular lines, 15–300 million of which are typically selected in a model. The equation of state is an extension of that used in Allard & Hauschildt (1995). For the coolest models the dust is assumed to form and to immediately rain out completely below the photosphere ('cond' models) so that it does not contribute to the opacity. Full details are available in Brott & Hauschildt (2005) and references therein.

Since we are working with dwarf stars, we assume $\log(g) = 5.0$ throughout. This assumption is in agreement with the values of $\log(g)$ determined from other techniques (Ségransan et al. 2003; Bean et al. 2006a; Berger et al. 2006). As we will see later, a change of ±0.5 dex in the assumed surface gravity implies only minor differences in the derived parameters.

The Phoenix models also include variations of α-elements for each metallicity. We have chosen to use models with no α-enhancement; in any case the use of α-enhanced models in dwarfs of earlier spectral type does not change the results significantly (Casagrande et al. 2006). There are indications that M dwarfs follow the same [α/Fe] versus metallicity as measured in FGK dwarfs (Woolf & Wallerstein 2005) and since our sample is limited to the solar neighbourhood we do not expect significant signs of α-enhancement.

3.1 Colour–colour plots

Testing of synthetic model atmospheres is normally done by comparing observed and modelled spectral energy distributions for a range of wavelengths and spectral types (e.g. Tinney, Mould & Reid 1993; Brett 1995b; Leggett et al. 1996, 2000, 2001; Burgasser, Cruz & Kirkpatrick 2007). Here we simply compare synthetic and empirical colours, showing that with good accuracy data right across the optical and IR, photometry provides an excellent tool to test model atmospheres (e.g. Bessell, Castelli & Plez 1998). The interested reader can find e.g. in Leggett et al. (2000, 2001) and Burgasser et al. (2007) a thorough discussion of the comparison and pitfalls between observed and modelled spectra for M dwarfs and subdwarfs.

Synthetic colours are computed from the model atmospheres using prescriptions very similar to those in Casagrande et al. (2006), as we discuss in more details in Appendix B. In Fig. 1 we plot various colour indices as function of $V - K_{\rm S}$. It is clear from the figure that the models have problems in $U - B$, being offset with respect to the observations by 0.1–0.2 mag. Such an offset is unlikely to be entirely due to uncertainties in standardize the U-band filter (see Appendix B) and/or the zero-points (as these amount to be at most 0.01–0.02 mag) and most likely reflects inadequacies in modelling the UV (ultraviolet) spectral region in cool stars. The models behave considerably better in the other optical and IR bands, although $J - H$ and $J - K_{\rm S}$ appear offset when going to dwarfs redder then $V - K_{\rm S} \gtrsim 5.5$ which corresponds to $T_{\rm eff} \lesssim 3000$ K (compare with Fig. 9).

Alternatively to $V - K_{\rm S}$, another excellent temperature indicator in cool stars is $I_{\rm C} - J$. In fact, Fig. 2 looks very similar to Fig. 1, but the stars are now distributed over a shorter baseline.

In the left-hand panel of Fig. 3 we show IR indices as function of $(R - I)_{\rm C}$, which is sensitive to decreasing spectral type for M dwarfs (Bessell 1991). The models are in fair agreement with the data, but get worse going to the reddest $(R - I)_{\rm C}$. Although at the very red end observed colours might be slightly less accurate (Section 2.1), Bessell (1991) has shown that the large spread in observed colours for the latest M dwarfs is real. The reason is likely to be that at such cool temperatures M dwarfs show the effects of dust at bluer wavelengths and have slightly different spectra with stronger hydride bands and weaker TiO and VO bands. In the purely IR colour planes of Fig. 3 we are working in narrow colour ranges and observational errors become prominent in the comparison. To help establish the trends we have also checked how these planes look when our sample of M dwarfs is complemented with the earlier one for G and K dwarfs from Casagrande et al. (2006). At bluer colours the data show a turnover in $J - H$ and $J - K_{\rm S}$ as function of decreasing temperature (i.e. increasing $H - K_{\rm S}$ and $I_{\rm C} - J$). The models partly predicted this feature, which is the result of the sensitivity of IR colours to the photospheric gas pressure (Mould 1976) as well as to the occurrence of H_2O bands. At very low effective temperatures, the data suggest a flattening and a possibly a rising in $J - H$ and $J - K_{\rm S}$, whereas the models decrease steadily. The rising of the observed colours in the $H - K_{\rm S}$ versus $J - H$ plane is confirmed by similar plot using dwarfs much cooler than we have here (e.g. Reid et al. 2001; Burgasser et al. 2007). This mismatch between data and models was already noticed in other models by Brett (1995b), and essentially means that in the models H and $K_{\rm S}$ magnitudes become progressively fainter than J magnitude as the effective temperature decreases.

Overall, the Phoenix models show fair agreement with the data in various bandpasses, although inadequacies still persist, especially at the coolest temperatures where the dust needs to be properly incorporated. The synthetic colours also show a large spread with metallicity for decreasing $T_{\rm eff}$: since our sample is limited to the solar neighbourhood, we expect our M dwarfs share a distribution

[1] The calibration of Bonfils et al. (2005) returns [Fe/H], whereas the model atmospheres are given for the total heavy elements fraction [M/H]. For low values of alpha-enhancement, the difference between the two is negligible, particularly since metallicity measurements in M dwarfs are still uncertain. In the rest of the paper we will refer to [M/H], although this is in practice [Fe/H] when we refer to empirical measurements.

[2] ftp.hs.uni-hamburg.de/pub/outgoing/phoenix/GAIA/

Downloaded from http://mnras.oxfordjournals.org/ by guest on January 20, 2015

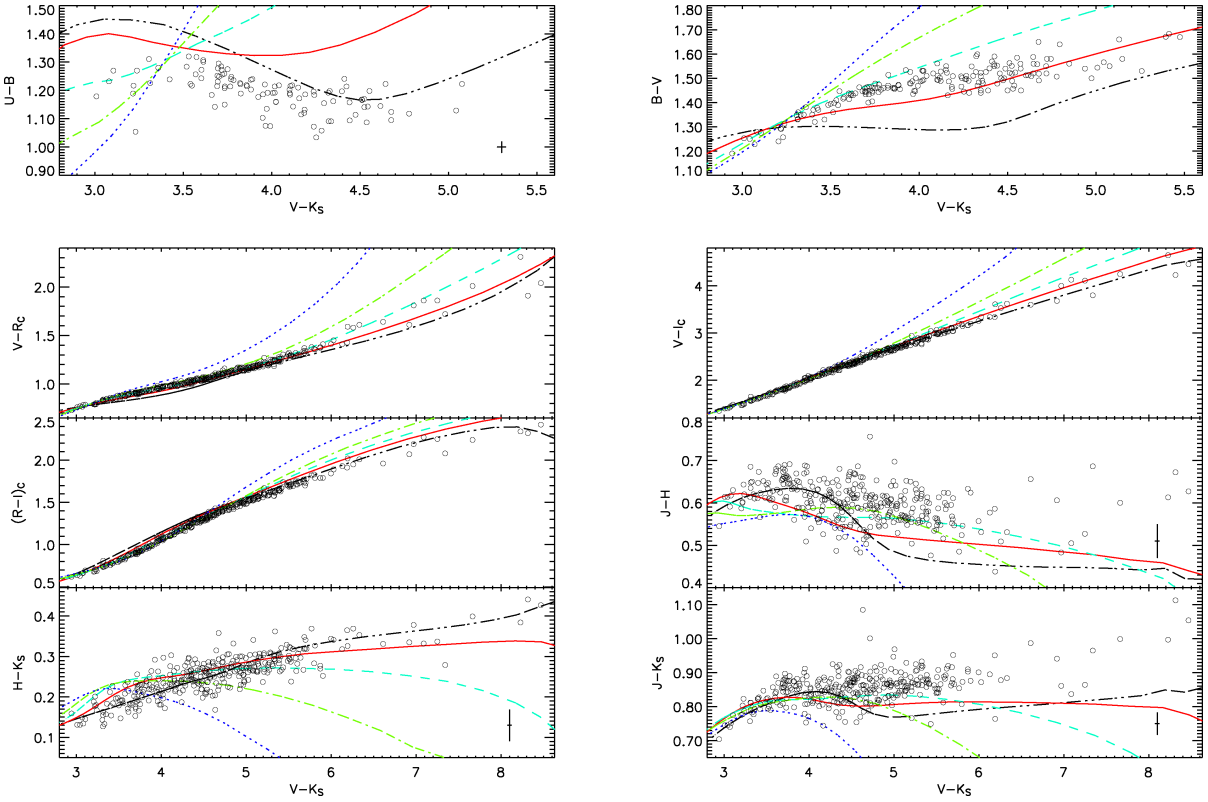

Figure 1. Synthetic optical and IR colours from the Phoenix models compared to our 343 sample stars of Section 2. Lines correspond to models with [M/H] equal +0.5 (double-dot–dashed), +0.0 (continuous), −0.5 (dashed), −1.0 (dot–dashed) and −1.5 (dotted). Since metallicities for M dwarfs are usually not available or are very uncertain, we have not used any metallicity bin for the stars (open circles). Typical error bars are shown only for certain indices; in the other bands error bars are comparable or smaller than the size of the plotting symbols, with very red stars (from Henry et al. 2004) which are somewhat less accurate.

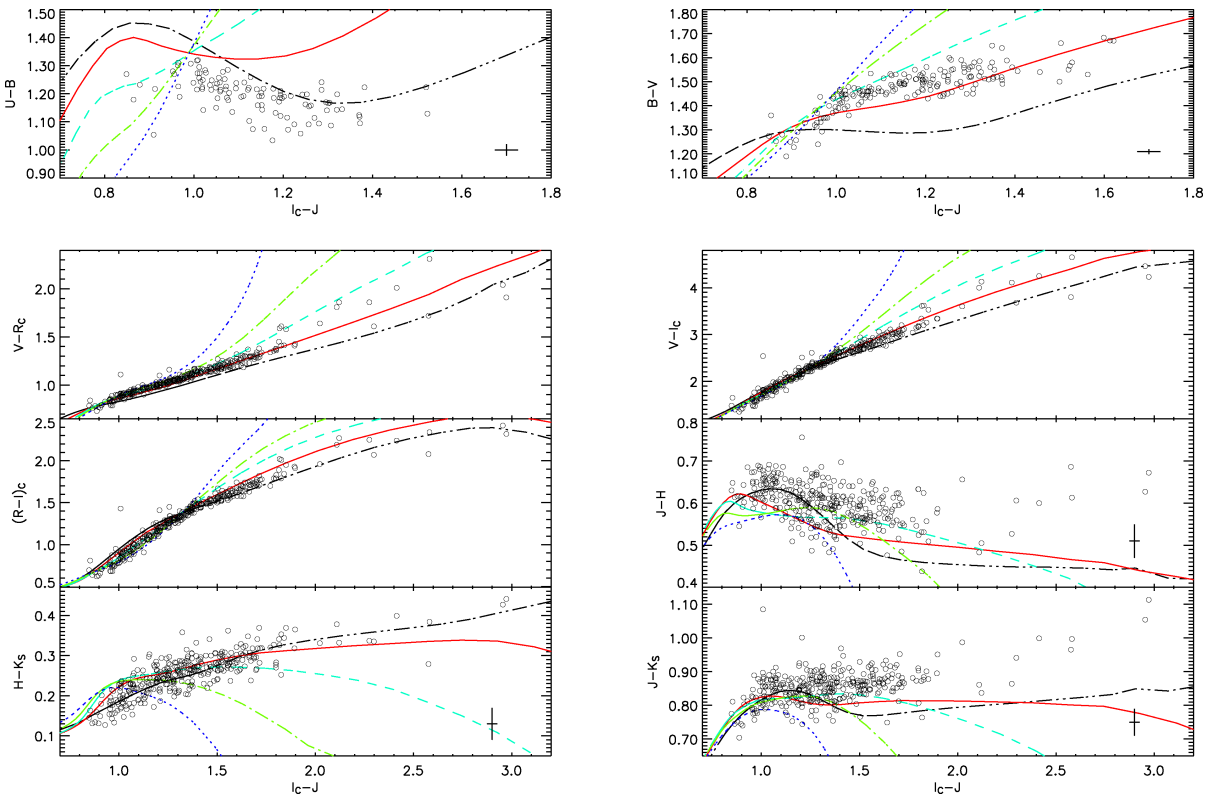

Figure 2. Same as Fig. 1 but as function of $I_C - J$ colour index.

Downloaded from http://mnras.oxfordjournals.org/ by guest on January 20, 2015

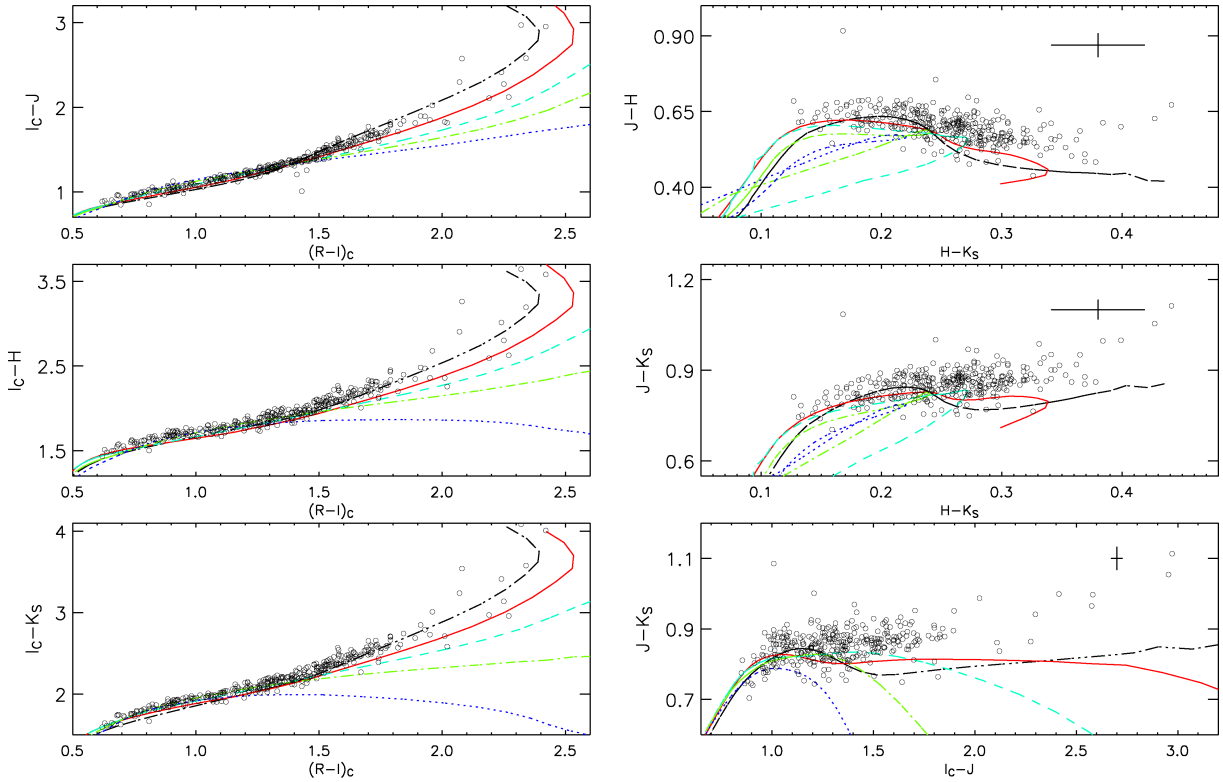

Figure 3. Same as Fig. 1 but as function of other colour indices.

similar to that observed in GK dwarfs, i.e. with most of the metallicities between −0.5 and 0.0. To this respect, the coolest models are considerably offset with respect to the position of the stars which are encompassed by supersolar and solar lines, rather than solar and subsolar as one would expect from the argument mentioned above. The serious discrepancies in *U* band have little impact on the present work of calibrating the bolometric luminosities of the stars, since so little flux is emitted in the *U* band. For the reddest stars, which correspond to effective temperatures below 3000–2900 K (see Fig. 9), the models do show some problems, especially in the IR. Since our technique partly relies on model atmospheres, this means that at the very cool end the results we present in Sections 5–7 are still open to refinements. Looking at Figs 1–3 is obvious that by simply comparing observed and theoretical colours one would deduce different stellar parameters (effective temperatures and metallicities) depending on the colour index adopted for the comparison. The technique we present in the next section is less affected by such inconsistencies. In fact, we will use model atmosphere only to estimate the flux outside our multiband photometry, i.e. the flux in the blue and red tails of the spectra. This estimate should be rather accurate as long as model atmosphere reproduce the overall spectral energy distribution, even though specific bands might have problems. Notice though, where theoretical models do show limitations, like in the optical and near-IR, we use anyway the observed colours. In addition, for estimating the metallicities we will calibrate our technique on other empirical measurements (see Section 5), and this should keep under control the deficiencies that still affect theoretical models. None the less, it would be too optimistic to believe we are not affected by the inaccuracies in the models. Future improvements on the theoretical side will certainly benefit to our technique, especially below 3000 K.

4 THE MULTIPLE OPTICAL–INFRARED TECHNIQUE

In our previous paper we used multiband photometry to implement the IRFM and we derived effective temperatures, bolometric luminosities and angular diameters for a set of G and K dwarfs (Casagrande et al. 2006). It is therefore natural to ask whether the same technique can be successfully applied to M dwarfs.

Although the underlying idea of the IRFM is still valid when going to effective temperatures cooler than ∼4000 K, some caveats exist. Here, we generalize and extend our temperature scale to dwarf stars much cooler than in Casagrande et al. (2006) to which the reader can refer for an introduction to the formalism and details on the computation of the bolometric and monochromatic flux from multiband photometry. The extension of the method presented here concerns the computation of $T_{\rm eff}$, which is now done by using the fluxes in both optical and IR bands (Section 4.2). For this reason we call our method the multiple optical–infrared technique (MOITE). As in Casagrande et al. (2006), the effective temperatures we derive depend on very few basic assumptions, namely the adopted Vega absolute calibration and zero-points (see also Appendix B). The dependence on the adopted grid of model atmospheres is also not so crucial since most of the bolometric flux (usually around 80 per cent) is recovered from our multiband photometry. The MOITE proves to be also sensitive to metal content in M dwarfs, as we discuss in Section 4.3.

4.1 The IRFM in brief

The basic idea of the IRFM (Blackwell & Shallis 1977; Blackwell, Shallis & Selby 1979; Blackwell, Petford & Shallis 1980) is to

Downloaded from http://mnras.oxfordjournals.org/ by guest on January 20, 2015

compare the ratio between the bolometric flux $\mathcal{F}_{\rm Bol}$(Earth) and the IR monochromatic flux $\mathcal{F}_{\lambda}$(Earth), both measured at Earth (the so-called observational $R_{\rm obs}$ factor) to the ratio between the surface bolometric flux ($\sigma T_{\rm eff}^4$) and the surface IR monochromatic flux $\mathcal{F}_{\lambda}$(model), predicted from model atmospheres. The ratio of the last two quantities defines the theoretical $R_{\rm theo}$ factor. From this ratio $T_{\rm eff}$ can be computed iteratively as follow:

$$T_{{\rm eff},n} = \left[\frac{\mathcal{F}_{\lambda}({\rm model})_{(n-1)}\mathcal{F}_{\rm Bol}({\rm Earth})_{(n-1)}}{\sigma\,\mathcal{F}_{\lambda}({\rm Earth})_{(n-1)}}\right]^{1/4}, \quad (1)$$

where the effective temperature determined at the nth iteration depends on the effective temperature determined at the $(n-1)$th iteration and which is used to improve the estimate of the quantities on the right-hand side of equation (1). In the IRFM, more than one IR band is usually used (i.e. $R_{\rm theo}$ is computed for each band), and the procedure described here is applied to each band separately. At each iteration the average $T_{{\rm eff},n}$ obtained from all the IR bands is then computed and the procedure is iterated until the effective temperature converges to a final value.

The IRFM has been traditionally applied to stars of K or earlier spectral type to derive effective temperatures approximately above 4000 K. Qualitatively, above this temperature, spectra roughly behave like blackbody curves in the IR, so that in this region the spectra can be described by the Rayleigh–Jeans law and the ratio between the bolometric and monochromatic flux depends on the effective temperature to some power, with little or no metallicity dependence (Fig. 4).

4.2 From the IRFM to the MOITE: a top level description of the technique

We now generalize the technique presented in the previous section to effective temperatures cooler than 4000 K using both optical and IR bands with the MOITE. We aim to give here a qualitative description of the underlying idea, leaving the full technical details to Appendix A.

Below approximately 4000 K, molecular absorption and flux redistribution become very important and significantly change the original continuum shape, making any type of qualitative blackbody description to an M dwarf spectrum hazardous also in the IR. Further, as the effective temperature decreases the peak of the spectra moves redward, until at $T_{\rm eff} \sim 3000$ K it settles in J band and stops moving further to the red (Allard & Hauschildt 1995). Below ∼4000 K, depending on the IR band, $R_{\rm theo}$ flattens out and then monotonically increases with decreasing effective temperature. This behaviour in the IR resemble that shown by $R_{\rm theo}$ also in the optical bands (Fig. 4).

It seems therefore obvious that below 4000 K, depending on the metallicity, particular care must be used in determining the effective temperature by means of the flux ratio. On the other hand, since in cool stars $R_{\rm theo}$ behaves qualitatively the same in both IR and optical colours, once a technique for determining $T_{\rm eff}$ is found, that can be readily applied to any photometric band.

As we discuss in more detail in Appendix A, when $R_{\rm theo}$ monotonically increases with decreasing temperature it is still possible to converge in $T_{\rm eff}$ if we compare the observed flux product $\mathcal{F}_{\rm Bol}$(Earth) × $\mathcal{F}_{\lambda}$(Earth) to its theoretical counterpart $(\theta/2)^4\sigma T_{\rm eff}^4 \mathcal{F}_{\lambda}$(model). The apparent drawback of this method is that it introduces a dependence on the angular diameter, whereas such a dependence was cancelled out when doing the flux ratio. However, at each nth iteration the angular diameter can be estimated from the $(n-1)$th iteration:

$$\left(\frac{\theta}{2}\right)_n^4 = \left[\frac{\mathcal{F}_{\rm Bol}({\rm Earth})_{(n-1)}}{\sigma\,T_{{\rm eff},n-1}^4}\right]^2, \quad (2)$$

so that it is still possible to converge in effective temperature:

$$T_{{\rm eff},n} = \left[\frac{\sigma\,\mathcal{F}_{\lambda}({\rm Earth})_{(n-1)}T_{{\rm eff},(n-1)}^8}{\mathcal{F}_{\rm Bol}({\rm Earth})_{(n-1)}\mathcal{F}_{\lambda}({\rm model})_{(n-1)}}\right]^{1/4}. \quad (3)$$

Since this formalism is valid when $R_{\rm theo}$ monotonically increases with decreasing temperature, the advantage of this approach is that

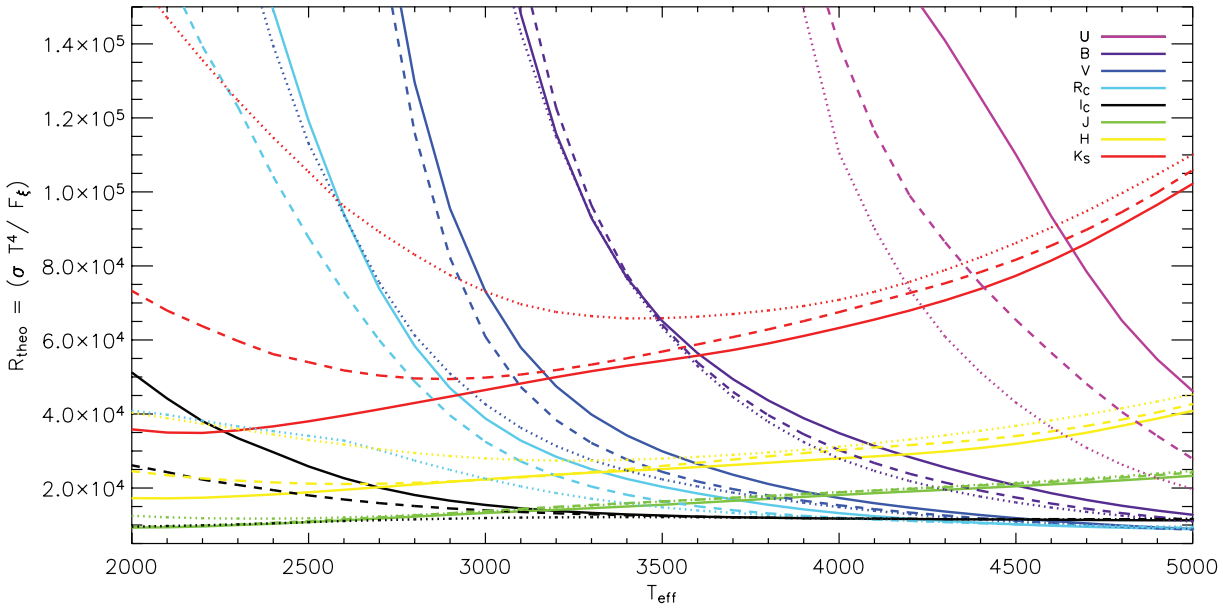

Figure 4. Ratio between the bolometric and the monochromatic flux ($R_{\rm theo}$) in various filter bandpasses ξ (lines of different colours) as function of $T_{\rm eff}$ for the Phoenix models in three different metallicities +0.0 (solid), −1.0 (dashed) and −2.0 (dotted). Broad-band (heterochromatic) fluxes have been reduced to monochromatic fluxes as described in the appendix B of Casagrande et al. (2006).

Downloaded from http://mnras.oxfordjournals.org/ by guest on January 20, 2015

now it is possible to use also the optical colours to converge in effective temperature below ∼4000 K. Notice that to bootstrap either the IRFM or the MOITE one needs to interpolate over a grid of synthetic spectra according to the details given in Appendix A. To do so, the metallicity of a star must be known: when this is not possible, [M/H] has been obtained with the procedure we describe in the next section.

4.3 Estimating the metallicities of M dwarfs with the MOITE

Fig. 4 shows that going to cooler $T_{\rm eff}$, both optical and IR colours start to show a strong dependence on the metallicity. We exploit this particularity to implement a novel technique to estimate the metallicities of the M dwarfs.

The method works as follows: for a given star of unknown metallicity, we apply the MOITE to recover the effective temperature, assigning each time a trial [M/H] to the star, from −2.1 to 0.4 dex, in steps of 0.1 dex. The trial metallicity assigned to the star is used for interpolating over the grid of model atmospheres. The chosen metallicity range well brackets our (rather local) sample of M dwarfs. For a given star we obtain six T_ξ which estimates $T_{\rm eff}$ from each of the colour bands individually $V(RI)_{\rm C}JHK_{\rm S}$, for each of the 26 different metallicity choices (from −2.1 to 0.4 dex). Since each band has a different sensitivity to the metallicity, the scatter among the six T_ξ is at a minimum when the correct metallicity is chosen, as we prove in the next section for a set of synthetic colours.

For real data, there is an additional complication. Empirically, for the 118 M dwarfs with known [M/H], we find that the temperature estimates in each band T_ξ are on average offset by a few 10s of K from the average $T_{\rm eff}$ with a dependence on both [M/H] and $T_{\rm eff}$. This offset might be ascribed to zero-point errors in the absolute calibration (see also figs 8 and 12 in Casagrande et al. 2006) and/or to systematics in the spectral library, or both. The computation of $\mathcal{F}_{\rm Bol}$(Earth) and $\mathcal{F}_\lambda$(Earth) from the observed multiband photometry depends on the adopted zero-points and absolute calibration (Casagrande et al. 2006). Although our adopted Vega absolute calibration has been thoroughly tested in both optical and IR bands via ground- (Tokunaga & Vacca 2005) and spaced-based (Bohlin & Gilliland 2004; Price et al. 2004; Bohlin 2007) measurements, uncertainties at the level of a few per cent are present and are almost certainly responsible for the systematic offsets of order 10s of Kelvin in T_ξ between different bands. Stars with different metallicity and effective temperature emit differently in a given ξ band; since the adopted absolute calibration and zero-points change the contribution of each ξ band into the final result, this explains why the offsets are function of [M/H] and $T_{\rm eff}$. We use the 118 M dwarfs for which we know their metallicities to correct these offsets in T_ξ obtained from each band. For the real stars, this reduces the scatter in temperatures for each of the trial metallicities, and considerably assists in the recovery of the correct metallicity. Notice that this correction to properly estimate [M/H] for our stars is calibrated on the Bonfils et al. (2005) metallicity scale, but for a given metallicity, $T_{\rm eff}$ is obtained with the MOITE alone.

4.4 MOITE: accuracy of the technique

The first test for the MOITE is to ensure that the proposed technique works, and if so, to which accuracy. The best way to address the level of internal accuracy of the method is by using synthetic colours to check whether the correct physical parameters (i.e. $T_{\rm eff}$ and [M/H]) of the underlying synthetic spectra are recovered.

We use the Phoenix model atmospheres to generate a set of synthetic $BV(RI)_{\rm C}JHK_{\rm S}$ magnitudes for stars in the temperature range $2100 \leq T_{\rm eff} \leq 4500$ K and metallicity range $-2.0 \leq$ [M/H] ≤ 0.0 dex. Notice that now the adopted absolute calibration and zero-points are not responsible for any offset among T_ξ in different bands, since the same absolute calibration and zero-points are used in generating synthetic magnitudes and in the MOITE.

We begin by applying the MOITE, regarding [M/H] as a fixed, known parameter. To get the iteration started, initial temperature estimates were made using Bessell (1991) $T_{\rm eff} : (R-I)_{\rm C}$ calibration. We find that we can recover the correct effective temperatures of the model spectra with an accuracy of 1 ± 3 K and the bolometric luminosities (i.e. $\sigma T_{\rm eff}^4$) within 0.1 per cent. We then tested what happens if rather than using the Bessell (1991) $T_{\rm eff} : (R-I)_{\rm C}$ calibration for the first estimate of the effective temperature we start either from $T_{\rm eff} = 5000$ K or from $T_{\rm eff} = 2000$ K. The method still recovers the correct temperatures and bolometric luminosities with the same accuracy as before (but more iterations are needed). The MOITE is thus pretty insensitive to poor first guesses of the effective temperature and always correctly converges.

We have then tested the MOITE at recovering metallicity (i.e. introducing [M/H] as a free parameter) as well as effective temperature and luminosity. We find we can recover the metallicities of the underlying synthetic spectra with an accuracy of 0.006 ± 0.04 dex, with very few cases when they deviate by 0.1 dex. As a consequence, $T_{\rm eff}$ and the bolometric luminosities are still recovered with very good accuracy. These tests establish that the technique has a high internal accuracy in the ideal case of no observational errors.

For a more realistic approach, we mimic real data by running Monte Carlo simulations with realistic observational uncertainties. For a set of synthetic $BV(RI)_{\rm C}JHK_{\rm S}$ colours, we have assigned each time random errors with a normal distribution centred on the synthetic values and a standard deviation equal to the typical optical (Section 2.1) and IR (Section 2.2) photometric errors. The results are shown in Fig. 5, and demonstrate that the method becomes more accurate when going to lower $T_{\rm eff}$, since at cool temperatures the flux ratios show a pronounced dependence on the metallicity as expected from Fig. 4. Now that realistic observational errors are taken into account we recover the metallicities of the synthetic spectra within 0.1–0.3 dex and the effective temperatures within 50–100 K, also depending on the spectral type. It is important to remember that real data might include systematic uncertainties (especially in the absolute calibration) which are difficult to assess and therefore not included when running the Monte Carlo simulations. The actual accuracy might be somewhat worse than in Fig. 5. Furthermore, it is fair to remember that the comparison with the observed colours (Section 3.1) shows that at coolest temperatures there is still room for improvements in theoretical modelling. For very cool stars, our results are therefore subject to possible refinements. However, even in the range $3000 < T_{\rm eff} < 4000$ K the method recovers [M/H] and $T_{\rm eff}$ of the underlying synthetic spectra with an accuracy of ∼0.2 dex and ∼50 K at a confidence level of 85 per cent (i.e. within 1.5σ).

We conclude that the MOITE shows a high degree of internal accuracy over the range of metallicities and effective temperatures covered in the present study. However, for a better estimate of the reliability of such a technique, we need to compare our results with direct measurements. This will be done in Sections 5 and 7 where we will compare the metallicities and the effective temperatures returned by the MOITE with those recently measured in literature by means of other techniques.

Downloaded from http://mnras.oxfordjournals.org/ by guest on January 20, 2015

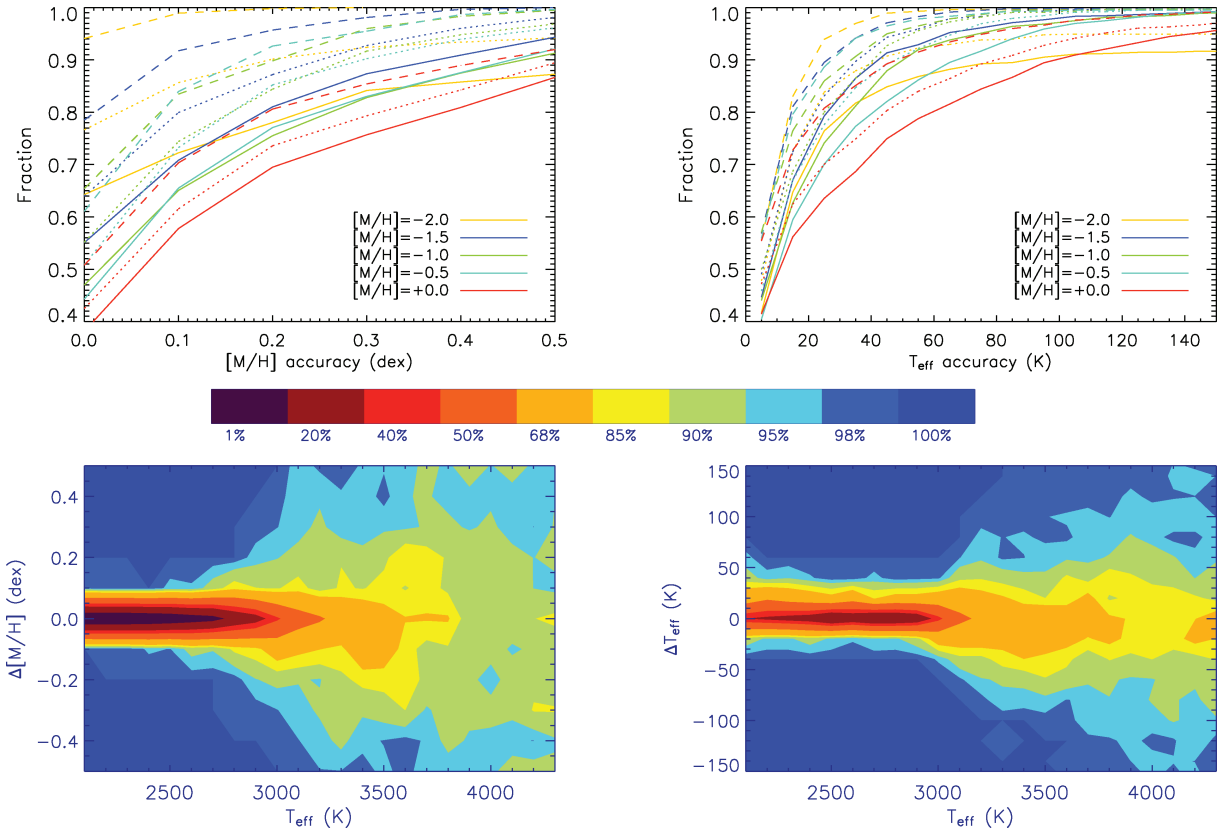

Figure 5. Upper panels: accuracy of the MOITE in recovering the correct [M/H] and $T_{\rm eff}$ when realistic observational uncertainties (Section 4.4) are included in the Monte Carlo simulation. Different line-styles correspond to the recovered parameters for $T_{\rm eff} \leq 4300$ K (continuous line), 3900 K (dotted) and 3500 K (dashed). Lower panels: contour plots showing the accuracy of the method as function of $T_{\rm eff}$. When going to cooler effective temperature the fluxes in different bands become extremely sensitive to the metal content and the physical parameters of the underlying synthetic spectra are always recovered with excellent accuracy, as discussed in the text.

4.5 The final error budget

We have shown our technique to be very promising in obtaining both effective temperatures and metallicities of cool stars. Based on the comparison with other measurements, in the next section we will estimate the uncertainty of our metallicities to be on average 0.2–0.3 dex especially when photometry is available in many bands.

For evaluating the final errors in effective temperatures, bolometric luminosities and angular diameters, we use the same prescriptions as in Casagrande et al. (2006). Briefly, for each star we run 200 Monte Carlo simulations assigning each time random errors to the photometry (according to the uncertainties given in Sections 2.1 and 2.2) and to [M/H]. We have also accounted for a change of ± 0.5 dex in the value of $\log(g)$ used in our grid of model atmospheres and for the case the errors in the absolute calibration correlate to give systematically higher or lower fluxes. When using the MOITE to estimate the metallicities, we search for the solution that minimize the scatter among T_{ξ}. Although the scatter is minimized, it is always finite: this reflects photometric errors as well as possible systematics which are not fully corrected, especially at the lowest temperatures. We adopt a very conservative approach and also include the scatter in different bands in the final $T_{\rm eff}$ uncertainty.

The effective temperatures, $m_{\rm Bol}$ and the metallicities for our entire sample are given in Table 1. On average, our effective temperatures are accurate to about 100 K which corresponds to

Table 1. Observable and physical quantities for our sample stars.

Name	$T_{\rm eff} \pm \Delta T_{\rm eff}$ (K)	$\theta \pm \Delta\theta$ (mas)	$m_{\rm Bol}$	V	$B-V$	$U-B$	$V-R_{\rm C}$	$V-I_{\rm C}$	J	H	$K_{\rm S}$	[M/H]
HIP 112	3923 ± 142	0.209 ± 0.016	9.668	10.748	1.410	1.320	0.879	1.722	8.017	7.408	7.217	−0.08
HIP 897	3786 ± 126	0.228 ± 0.016	9.628	10.822	1.463	1.249	0.914	1.826	7.976	7.314	7.119	−0.18
HIP 1734	3397 ± 154	0.306 ± 0.029	9.459	11.133	1.508	1.162	1.009	2.209	7.674	7.052	6.785	0.07
HIP 1842	3327 ± 110	0.241 ± 0.017	10.073	11.886	1.523	1.166	1.042	2.326	8.259	7.640	7.375	0.04
...	...	...	...	...	...	...	...	...	...	...	...	...

Effective temperatures ($T_{\rm eff}$) and angular diameters (θ) are computed as described in the text. For the stars with HIP number, the metallicities are from the Bonfils et al. (2005) calibration, while the remainder are obtained with the MOITE. We only give metallicities for stars with $T_{\rm eff}$ above 3080 K for the reasons explained in Section 5. Apparent bolometric magnitudes ($m_{\rm Bol}$) are obtained according to Section 6, where the absolute bolometric magnitude of the Sun $M_{\rm Bol,\odot} = 4.74$. Optical colours are in the Johnson–Cousins system, whereas IR are from 2MASS. The full table is available in the online version of the article.

Downloaded from http://mnras.oxfordjournals.org/ by guest on January 20, 2015

2–3 per cent in the studied temperature range. The uncertainty in bolometric luminosities is usually between 3 and 4 per cent and that in angular diameters between 4 and 6 per cent. Furthermore, the fact that the MOITE recovers the metallicities consistently with other determinations, although is not a proof of the correctness of $T_{\rm eff}$ is reassuring and indirectly confirms the accuracy of the temperatures (Fig. 5).

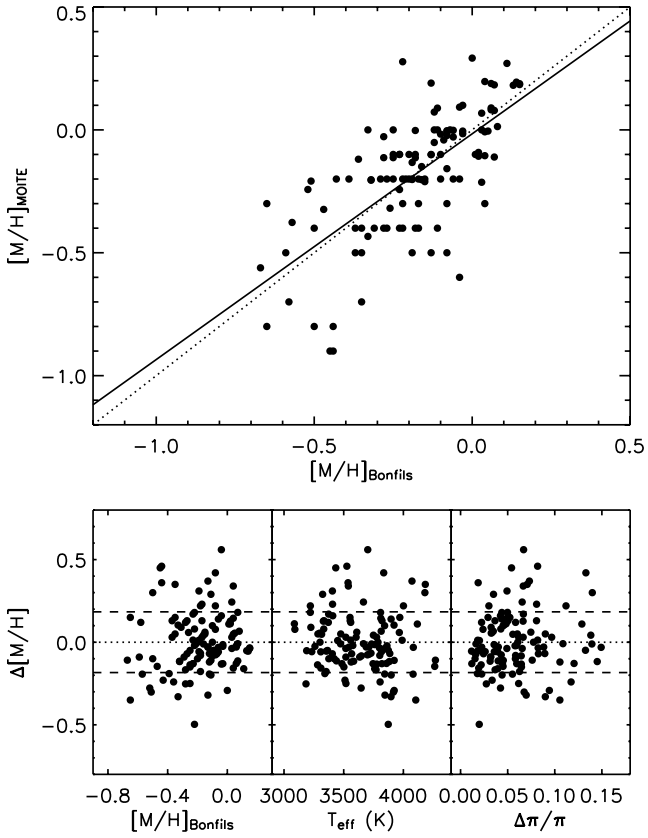

Figure 6. Upper panels: comparison between the Bonfils et al. (2005) metallicities and those obtained with the MOITE. The continuous line is the fit to the data, the dotted line is the one-to-one relation. Lower panels: the metallicity difference ([M/H]$_{\rm Bonfils}$ − [M/H]$_{\rm MOITE}$) as function of other parameters. Long-dashed lines are the 1σ scatter.

5 THE M DWARF METALLICITY SCALE

In the previous section we have introduced how the MOITE works and we have evaluated its accuracy by means of Monte Carlo simulations. Here, we compare the metallicities obtained with our technique to those recently measured by Bonfils et al. (2005), Woolf & Wallerstein (2005, 2006), Bean et al. (2006a) and Bean, Benedict & Endl (2006b). For dwarfs with $T_{\rm eff}$ below 3000 K we use *Hipparcos* common proper motion companions to compare the metallicity we derive for the cool secondaries with that more easily measured for the hotter primaries in the aforementioned studies. We will compare our effective temperatures with other determinations available in the literature in Section 7.

5.1 Accuracy of the metallicities above 3000 K

Fig. 6 shows our metallicity estimates for the 118 M dwarfs with known metallicities, and shows a 1σ scatter of 0.2 dex, i.e. within the accuracy of the Bonfils et al. (2005) calibration. This comparison is encouraging, but still includes stars which were used to construct the calibration (Section 4.3), so is not a fully external check on the method.

Recently, reliable metallicities for M dwarfs have been measured by Woolf & Wallerstein (2005, 2006) from very high resolution spectra. Spectral synthesis technique has been also successfully applied by Bean et al. (2006a,b). We have extensively searched for $BV(RI)_{\rm C}JHK_{\rm S}$ photometry of M dwarfs analysed in the aforementioned studies and found accurate measurements for those reported in Table 2: for $T_{\rm eff}$ approximately above 3000 K the mean difference in metallicity is just -0.03 ± 0.06 dex ($\sigma = 0.17$ dex). In particular, the comparison with the direct spectroscopic measurements of Woolf & Wallerstein (2005, 2006) agrees always within 0.13 dex (filled diamonds in Fig. 7). The agreement with the [M/H] measurements of Bean et al. (2006a,b) is somewhat poorer (asterisks in Fig. 7), but there are large discrepancies between their and our $T_{\rm eff}$ scale, as we discuss later in this section. Such large differences in the adopted $T_{\rm eff}$ obviously reflect in the abundances measured by Bean et al. (2006a,b).

Notice that our technique relies on the metallicities determined from Bonfils et al. (2005), whose calibration also includes measurements from Woolf & Wallerstein (2005). To further and independently test our results, we have applied the MOITE to all the stars in Woolf & Wallerstein (2006). For these stars, only $VJHK_{\rm S}$ photometry is available. We have used V magnitudes as given in table 1

Table 2. Magnitudes and colours for various M dwarfs and the $T_{\rm eff}$ and [M/H] recovered with the MOITE compared with those obtained by other techniques. In the IR we have used $JHK_{\rm S}$ magnitudes from 2MASS.

Name	NLTT	V	$B-V$	$V-R_{\rm C}$	$V-I_{\rm C}$	Ref.	$T_{\rm eff}^{\rm MOITE}$ (K)	[M/H]$_{\rm MOITE}$	$T_{\rm eff}$ (K)	[M/H]$_{\rm meas.}$	Ref.
GJ 191	14 668	8.841	1.570	0.956	1.951	1	3661	−1.00	3570	−0.99	a
GJ 701	45 883	9.362	1.515	0.976	2.060	2	3557	−0.20	3630	−0.20	a
GJ 828.2	51 282	11.090	1.534	0.964	1.967	2	3646	−0.24	3680	−0.37	b
GJ 876	55 130	10.179	1.571	1.182	2.733	2	3076	−0.09	3478	−0.12	c
GJ 581	39 886	10.568	1.602	1.109	2.501	2	3211	0.00	3480	−0.33	c
GJ 297.2 B	19 072	11.80	1.49	1.03	2.29	4	3370	−0.20	3659	−0.12	d
GJ 105 B	8 455	11.66	1.50	1.22	2.78	4	3048	−0.30	3444	−0.09	d
GJ 412 B	26 247	14.44	2.08	1.66	3.77	3	2700	−0.31	–	−0.43	a
GJ 618 B	42 494	14.15	1.79	1.412	3.233	3	2614	−0.26	–	−0.12	e
GJ 752 B	47 621	17.20	–	2.10	4.36	3	2250	−0.04	–	−0.04	e

Source of the optical photometry: 1 – Kilkenny et al. (1998); 2 – Koen et al. (2002); 3 – Bessell (1990a); 4 – Laing (1989). Source of metallicity: a – Woolf & Wallerstein (2005); b – Woolf & Wallerstein (2006); c – Bean et al. (2006b); d – Bean et al. (2006a); e – Bonfils et al. (2005). For the Bonfils et al. (2005) calibration we have used the V magnitudes given in the table and the $K_{\rm S}$ magnitudes from 2MASS.

© 2008 The Authors. Journal compilation © 2008 RAS, MNRAS **389,** 585–607

Downloaded from http://mnras.oxfordjournals.org/ by guest on January 20, 2015

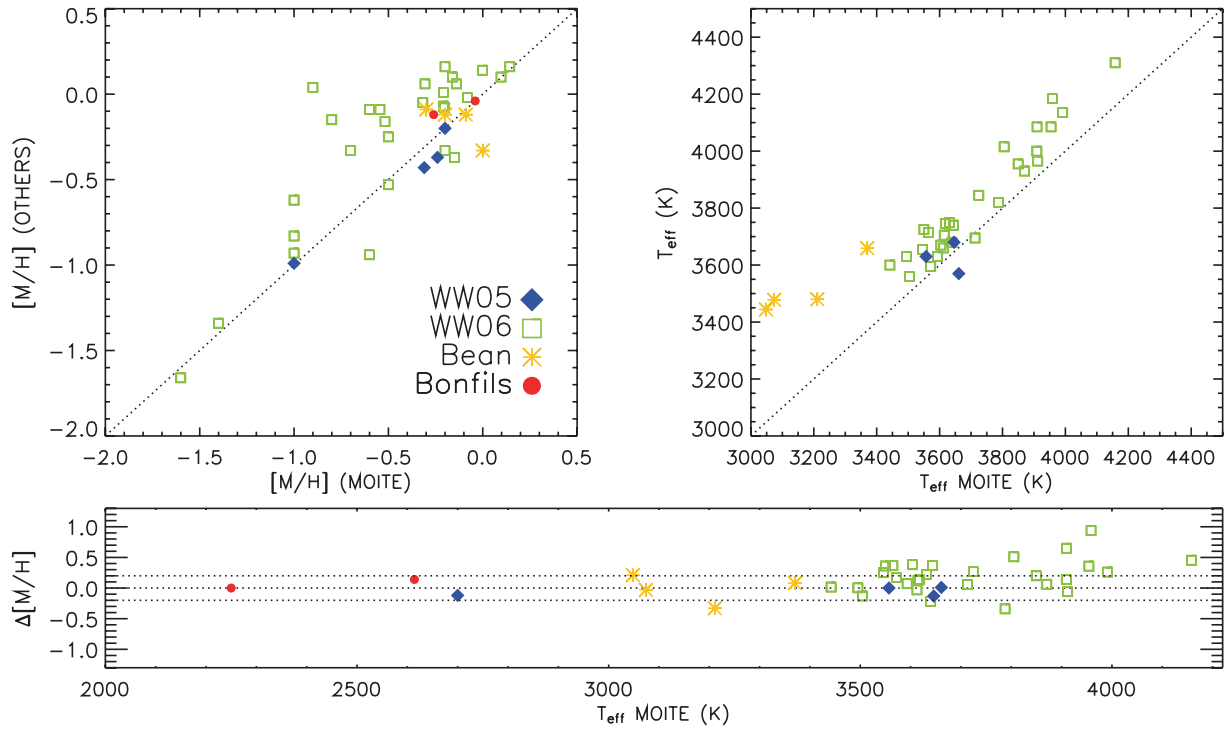

Figure 7. Comparison between $T_{\rm eff}$ and [M/H] obtained by the MOITE and those measured from Woolf & Wallerstein (2005) (filled diamonds), Woolf & Wallerstein (2006) (open squares), Bean et al. (2006a,b) (asterisks) and Bonfils et al. (2005) (filled circles) according to the details given in Sections 5.1 and 5.2. Notice that below 3000 K the metallicities are those measured in the *Hipparcos* common proper motion companions. In the first and second panel, dotted diagonal lines with slope 1 are intended to guide the eye. The horizontal dotted lines in the third panel highlight the $\pm$0.2-dex interval around the mean zero. Δ[M/H] refers to the difference $[{\rm M/H}]_{\rm others} - [{\rm M/H}]_{\rm MOITE}$.

of Woolf & Wallerstein (2006) and $JHK_{\rm S}$ from 2MASS. Again, we have used only stars with total photometric errors in the IR smaller than 0.10 mag. Since we are now running the MOITE using fewer colours, we might expect our results to be slightly less accurate. The comparison with the Woolf & Wallerstein (2006) measurements in Fig. 7 is reassuring, with a mean difference of 0.20 ± 0.05 dex ($\sigma = 0.27$ dex) and it validates our technique over a larger range of metallicities.

Differently from the study of FGK dwarfs, M dwarfs exhibit complex spectra which render far less trivial the determination of both effective temperatures and metallicities from spectroscopic analysis only. The purpose of this section is to evaluate the accuracy of our metallicities, whereas we compare our temperature scale with other existing ones in Section 7. It is however worth discussing here the differences with the effective temperatures adopted by Woolf & Wallerstein (2005, 2006) and Bean et al. (2006a,b) to derive their metallicities. Our effective temperatures are systematically cooler than those of Woolf & Wallerstein (2006), especially for earlier M spectral types (3700 K and above), where the difference in metallicities is also higher. Woolf & Wallerstein (2005, 2006) estimate $T_{\rm eff}$ from theoretical colour–temperature relations in $V-H$ and $V-K_{\rm S}$ obtained using older model atmospheres (Hauschildt et al. 1999a). According to Woolf & Wallerstein (2006), systematics as high as 100–200 K in their $T_{\rm eff}$ could not be excluded. Our effective temperatures are in agreement with the latest Phoenix and above 3500 K Castelli & Kurucz (2003) models, as it can be seen from Fig. 9. The disagreement in $B-V$ for the Castelli & Kurucz (2003) models is likely due to pitfall in accounting the contribution of all molecular features in these spectral regions. The effective temperatures obtained by the spectral fitting technique of Bean et al. (2006a,b) rely particularly on the TiO bandhead. Bean et al. (2006a) also notice that while at M0.5 spectral types their $T_{\rm eff}$ agree with the scale of Reid & Hawley (2005), their effective temperatures increase linearly with spectral type and for their latest M dwarf (GJ 105 B) they are about 300 K hotter than Reid & Hawley (2005) scale and 400 K hotter than our scale. This hotter temperature scale is possibly related to drawback in determining effective temperatures via spectral synthesis of certain bandhead (e.g. Jones et al. 2005). We will further discuss and test our temperature scale with other recent determinations, in particular with interferometric angular diameters, in Section 7 and prove our effective temperatures to be reliable.

Concluding, the metallicities estimate with the MOITE above $\sim$3000 K agree within 0.2–0.3 dex to those measured by other recent studies, especially when all $BV(RI)_{\rm C}JHK_{\rm S}$ photometry is available. In particular, the comparison with direct spectroscopic measurements of Woolf & Wallerstein (2005) suggests an even better agreement, at the level of 0.1 dex.

5.2 Accuracy of the metallicities below 3000 K

As we have already mentioned, the calibration performed in Section 4.3 is function of $T_{\rm eff}$ and [M/H] and in our case is obtained in the metallicity and temperature range shown in Fig. 6. The comparison in Fig. 7 suggests that the technique can be safely applied to metallicities as low as about -2.0 dex, at least above 3500 K and to metallicities typical of the solar neighbourhood down to about 3000 K. Here, we would like to test to what extent we can use the MOITE to measure metallicities in stars with effective temperatures below this latter limit. The extrapolation to lower temperatures is

Downloaded from http://mnras.oxfordjournals.org/ by guest on January 20, 2015

particularly interesting, since on the basis of our Monte Carlo simulations the MOITE is expected to recover the metallicity to high accuracy (always within 0.1–0.2 dex) below 3000 K (Fig. 5). Furthermore, for the coolest effective temperatures, as we discussed in Section 3.1, theoretical models do show discrepancies with respect to the empirical colour–colour diagrams. Those could reduce the formal high accuracy expected for $T_{\rm eff} < 3000$ K, so that below this temperature it is interesting to compare our with respect to other more 'direct' metallicity estimates.

We are not aware of any [M/H] measurement for M dwarfs with $T_{\rm eff} < 3000$ K, but from the list of Gould & Chanamé (2004), we have searched for multiband optical and IR photometry of late M dwarfs which are common proper motion companions to *Hipparcos* stars. We have then compared our metallicities estimated with the MOITE to those more easily measured for the primary *Hipparcos* stars. We have found three late M dwarfs (GJ 412 B, GJ 618 B, GJ 752 B) whose common proper motion companions are early-type M dwarfs with metallicities from Woolf & Wallerstein (2005) or from the calibration of Bonfils et al. (2005). We caution that some of the stars in Table 2 are classified as 'variable' in SIMBAD and GJ 618 B has very large photometric errors in 2MASS (much larger than our usual fiducial level 'j_', 'h_' and 'k_msigcom' < 0.10 mag).

There are only three stars and it is hard to draw definitive conclusions, but it is reassuring to see such a nice agreement, with the metallicity of the secondaries in agreement with that of the primaries within 0.14 dex even in the worst case. For two stars [M/H] of the primary is obtained using the Bonfils et al. (2005) formula, which we have used to calibrate our technique. None the less, now we are working with effective temperatures much cooler than those of Fig. 6 and the metallicities are still properly recovered. Of course more stars are needed before confidently extend our technique to such cool stars, but the method looks promising. To be on the safe side, for our entire sample of M dwarfs (Table 1) we give [M/H] only for stars with $T_{\rm eff}$ above 3080 K, i.e. only where the MOITE is safely calibrated as explained in Section 4.3.

6 EMPIRICAL BOLOMETRIC CORRECTIONS

We adopt the same definition of Casagrande et al. (2006) to define the bolometric correction in a given ξ band, where

$$\mathrm{BC}_{\xi} = m_{\rm Bol} - m_{\xi} \tag{4}$$

and the zero-point of the $m_{\rm Bol}$ scale is fixed by choosing $M_{\rm Bol,\odot} = 4.74$. Although it is possible to give analytic transformations between the flux and various colour indices, bolometric corrections can be readily computed using equation (4) in any band from the stars in Table 1, and are probably more useful.

The bolometric correction in V and R bands as function of various colour indices are shown in Fig. 8. In the optical there is some dependence on the metallicity among the coolest stars, but when going to longer colour baselines, the data show very tight relations, especially in $V - J$. The flux emitted by cool stars peaks in the near-IR. The bolometric corrections in $I_{\rm C}, J, H$ and $K_{\rm S}$ are almost constant as function of different colour indices. For these bands it is therefore possible to pass directly from the observed m_{ξ} to the bolometric magnitude $m_{\rm Bol}$ via linear fit as shown in Fig. 8 and given here:

$$m_{\rm Bol} = \begin{cases} 1.46 + 0.90\, m_{I_{\rm C}}, \\ 1.22 + 1.07\, m_{J}, \\ 1.94 + 1.06\, m_{H}, \\ 2.07 + 1.08\, m_{K_{\rm S}}. \end{cases} \tag{5}$$

Of course, by using the data in Table 1 to fit the bolometric correction as function of a given colour index it is possible to achieve higher accuracy still. None the less, the linear fits in Fig. 8 are useful to have a quick estimate of the bolometric magnitude given the apparent one. From these bolometric corrections and the colour–temperature relations given in the next section it is also possible to obtain very accurate estimates of the angular diameter of M dwarfs, as we describe in Section 7.1.

7 THE M DWARFS TEMPERATURE SCALE

We have fitted the observed colour–$T_{\rm eff}$ relations by analytical fits, using the following functional form:

$$\theta_{\rm eff} = a_0 + a_1 X + a_2 X^2 + a_3 X^3, \tag{6}$$

where $\theta_{\rm eff} = 5040/T_{\rm eff}$, X represents the colour and $a_i (i = 0, 1, 2, 3)$ are the coefficients of the fit. Depending on the band (Fig. 9), the data show an increasing scatter in the effective temperature estimates below ~2800 K, which is very likely due to metallicity dependencies. Because of this, we strongly caution against using $V - R_{\rm C}$, $V - I_{\rm C}$ and $(R - I)_{\rm C}$ indices below 2800 K. We have also verified that such scatter at low temperatures is not present in the other transformations of Table 3. We do not have enough stars below this temperature to address the question further and the metallicity estimates are still somewhat uncertain so that we do not include any metallicity dependence in our analytic fits. Furthermore, our M dwarfs are drawn from the solar neighbourhood, and they have a limited range of metallicities. It will be interesting to try the method on halo M dwarfs, as these become available especially in large photometric/spectroscopic surveys currently underway [e.g. from RAVE (Radial Velocity Experiment), SEGUE (Sloan Extension for Galactic Understand and Evolution), SkyMapper) and later with GAIA. We thus differ from the Casagrande et al. (2006) fitting formulae, which accounted for the larger metallicity coverage of that sample. Furthermore, now we need to fit a third-order polynomial to account for the inflection that occurs at lower $T_{\rm eff}$. For this reason, the fitting formulae of Table 3 are not an exact continuation of those in Casagrande et al. (2006), which are correct for $T_{\rm eff}$ hotter than 4400 K. Therefore, the colour ranges for the fits in Table 3 do not overlap with Casagrande et al. (2006), but are given for slightly redder colours. If a link between the two scales is needed, however, we advise the users to a careful case-by-case study.

With the exception of $B - V$, none of the colour–temperature transformations has strong dependence on [M/H] above 2800 K, and therefore our relations are not likely to be affected much as metallicities for M dwarfs improve. The temperature fit to the $B - V$ colour has huge scatter, and gives only the crudest temperature estimate. If one really needs to estimate $T_{\rm eff}$ from $B - V$ the best choice is probably to use Fig. 9.

We have searched for DENIS (Deep Near-Infrared Survey) photometry so as to give in Table 3 the colour–$T_{\rm eff}$ relations also in this system, although for a smaller number of stars. According to the DENIS data base, those magnitudes have larger photometric errors (on average between 0.05 and 0.09 mag) than 2MASS so this might explain why the relations in Table 3 are less accurate for the DENIS colours. Furthermore, we have found relations involving the $I_{\rm DENIS}$ very noisy and we do not give them.

For most of the stars in Koen et al. (2002) SAAO *JHK* photometry is also available from Kilkenny et al. (2007) and in Table 3 colour–temperature relations are given in this system, too. Stars with SAAO IR photometry are all hotter than 3000 K and because of the reduced temperature range, second-order polynomial fits are

Downloaded from http://mnras.oxfordjournals.org/ by guest on January 20, 2015

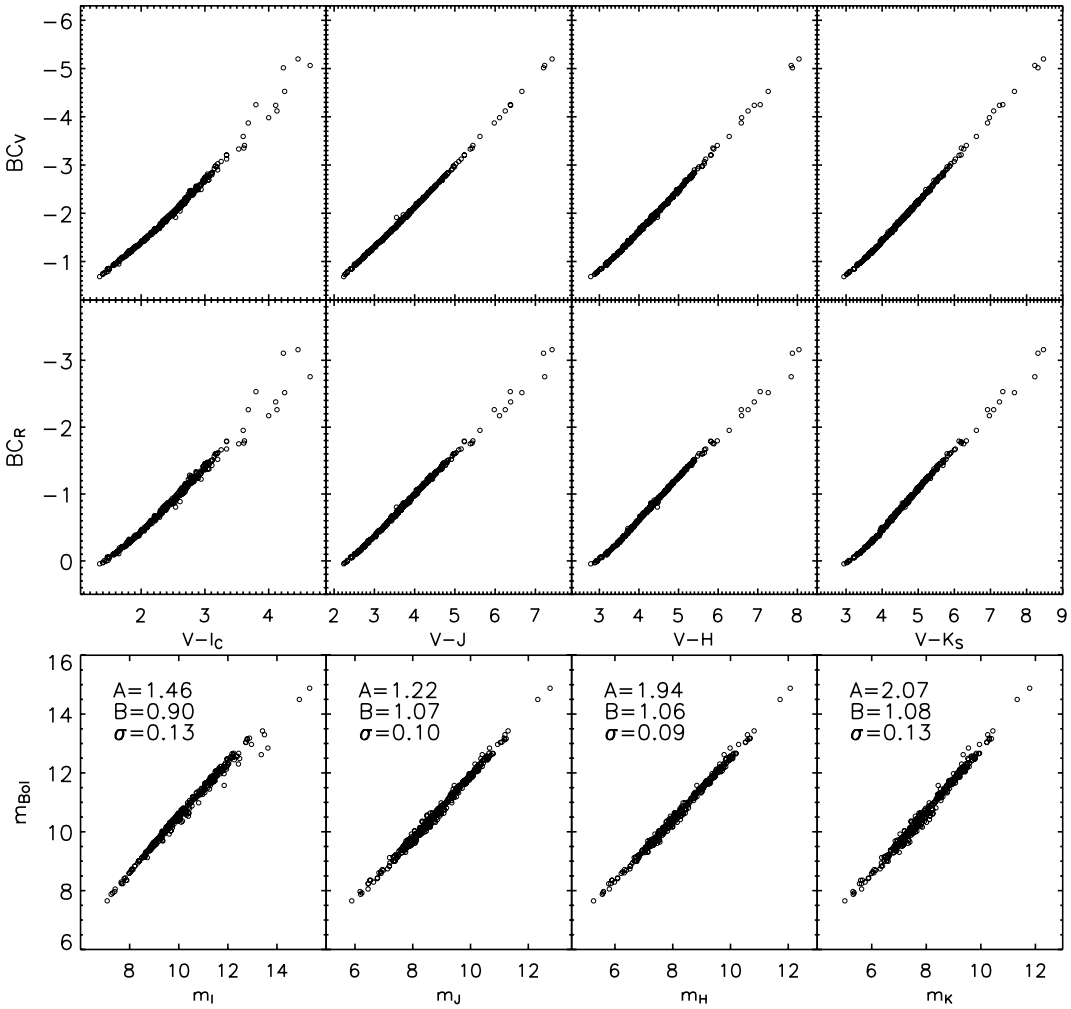

Figure 8. Upper and central panel: bolometric corrections in V and R bands as function of various colour indices for our M dwarfs. Lower panel: relation between the magnitudes observed in different bands m_ξ and the bolometric magnitude $m_{\rm Bol}$. Linear fits in the form $m_{\rm Bol} = {\rm A}+{\rm B}\,m_\xi$ are given along with the resulting standard deviation σ.

accurate enough now. We caution against extrapolating these relations to cooler temperatures, in particular for indices $I_{\rm C} - J_{\rm SAAO}$, $I_{\rm C} - H_{\rm SAAO}$ and $I_{\rm C} - K_{\rm SAAO}$.

Many M dwarfs are intrinsically variable, owing to spots or other activity. We have cleaned the sample from variable stars as best we can (and indeed our colour–temperature relations are very tight), however, there might still be unrecognized long-term variables present. The relations we give thus apply also to intrinsically low variability stars.

For the sake of completeness, we have applied the MOITE to the M dwarfs labelled as variable in the original Koen et al. (2002) sample and which were excluded, according to the selection criteria of Section 2. The stars were found to follow the same mean locii of the colour–temperature relations as the non-variables, but with a larger scatter, usually about twice the $\sigma(T_{\rm eff})$ of Table 3. One should keep in mind that the stars in Koen et al. (2002) were already preselected in *Hipparcos* in order to exclude extremely active stars: how well our results would apply to these latter objects we leave to future studies.

The latest Phoenix model atmospheres show good agreement with our colour–temperature relations in Fig. 9. This partly reflects the fact that our scale has been obtained using these models in the MOITE, but we are using a great deal of observational information to recover the total bolometric luminosity, and the model atmospheres are used only to estimate the missing flux, which is at most of order 20 per cent. We demonstrate further the reliability of our temperature scale in what follows: in Section 7.1 using recent determinations of angular diameters for M dwarfs, and in Section 7.2 comparing our results with those obtained by various recent temperature studies.

7.1 MOITE versus interferometric angular diameter measurements

Although in the past, much work has been done in determining the effective temperature scale of the M dwarfs, a firmly established scale has not been achieved. Until recently, in fact, the only two M dwarfs with measured linear diameters were the eclipsing binaries, YY Gem (Kron 1952; Habets & Heintze 1981) and CM Dra (Lacy 1977; Metcalfe et al. 1996), but the limiting factor in accurately determining their effective temperatures was the parallaxes. Long-baseline interferometry has recently provided angular diameters measurements for a handful of nearby M dwarfs which can be used to test the accuracy of our effective temperature and

Downloaded from http://mnras.oxfordjournals.org/ by guest on January 20, 2015

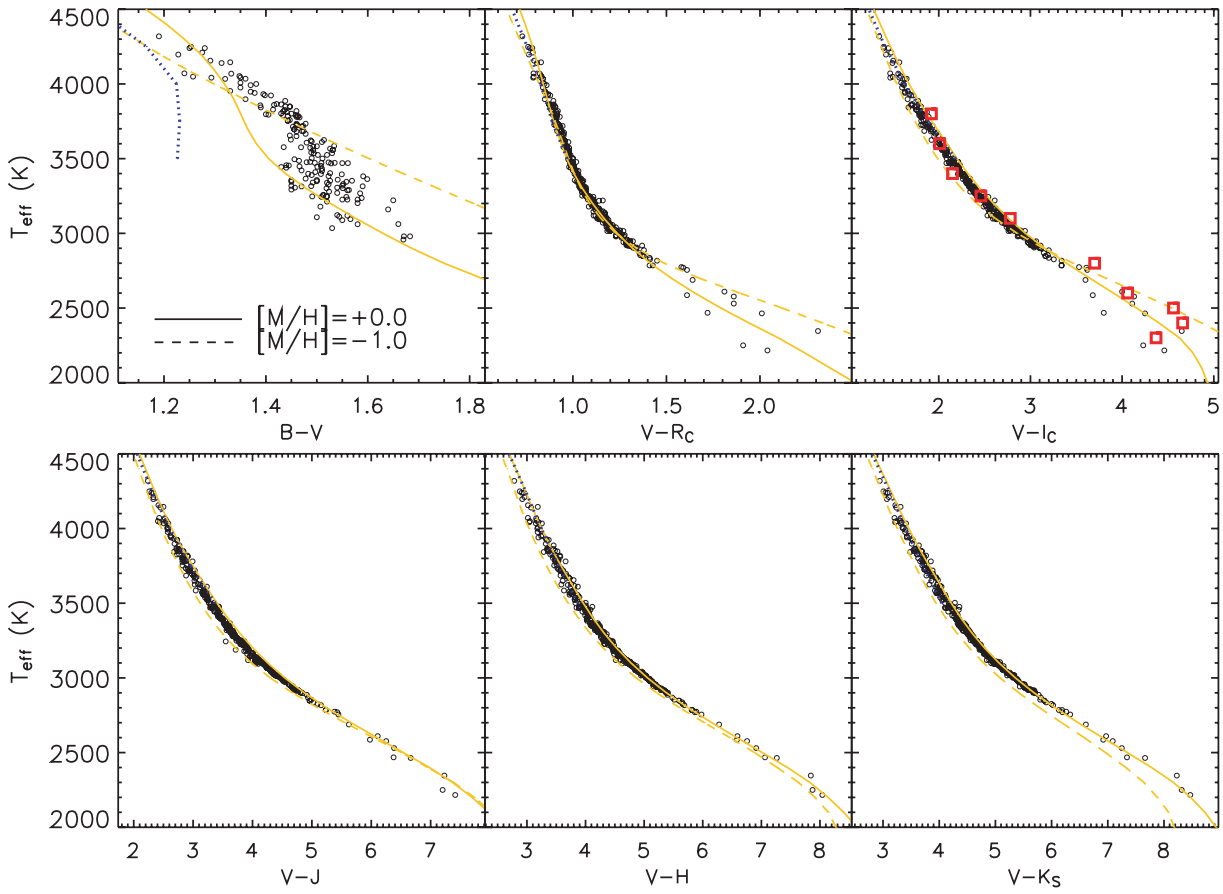

Figure 9. Colour–$T_{\rm eff}$ plots in different bands for our M dwarfs. Overplotted are the prediction from the Phoenix models (solid and dashed lines) for two different metallicities which roughly bracket our sample of stars. Also shown for comparison the prediction from the Castelli & Kurucz (2003) models for solar metallicity (dotted line). Squares in the $T_{\rm eff}$ versus $V-I_{\rm C}$ plot are from the temperature scale of Reid & Hawley (2005).

bolometric luminosity scale (Ségransan et al. 2003; Berger et al. 2006). Unlike G and K dwarfs, for which all the interferometric targets had saturated 2MASS photometry (Casagrande et al. 2006), half of the M dwarfs with measured angular diameters have good 2MASS colours.

The stellar angular diameters obtained with the MOITE are computed from the basic definition

$$\mathcal{F}_{\rm Bol}({\rm Earth}) = \left(\frac{\theta}{2}\right)^2 \sigma T_{\rm eff}^4, \qquad (7)$$

so that in principle a conspiracy of wrong effective temperatures and bolometric luminosities could still return correct angular diameters. However, the bolometric luminosities of our targets are observed via multiband photometry (only subject to minor corrections to estimate the missing flux, see also Appendix A), so that $\mathcal{F}_{\rm Bol}$(Earth) is fixed by the observations and therefore comparison of our angular diameters with those measured by interferometers automatically tests our temperature scale.

We caution that even interferometric angular diameter measurements depend mildly on modelling assumptions, in particular the limb-darkening corrections to convert the measured uniform-disc angular diameters into the physical limb-darkened discs ($\theta_{\rm LD}$) and to which we compare our θ of equation (7). The limb-darkening coefficients used for M dwarfs (Claret 2000) are computed using solar abundance atmospheric models, whereas the interferometric targets of Table 4 span a larger metallicity range. Another source of uncertainty is due to the fact that limb-darkening coefficients are calculated using one-dimensional (1D) atmospheric models, whereas three-dimensional (3D) models predict a less significant centre-to-limb variation. Such a difference might be up to a few per cent in $\theta_{\rm LD}$ for hotter F and G stars, but is expected to be much smaller in the case of M dwarfs (Allende Prieto et al. 2002; Bigot et al. 2006). Since all interferometric measurements reported here have been performed in the IR, where limb-darkening effects are minimized, we expect these uncertainties to be within the observational errors.

When running the MOITE for M dwarfs in Table 4 with good 2MASS photometry we have used the metallicities from Woolf & Wallerstein (2005) or applied the Bonfils et al. (2005) calibration, except for GJ 699 which is outside of the Bonfils' et al. (2005) range of applicability and for which a solar metallicity is thought to be appropriate (Leggett et al. 2000; Dawson & De Robertis 2004). The errors have been computed as described in Section 4.5. For the other stars (i.e. those with inaccurate 2MASS photometry) we apply the bolometric luminosity and effective temperature calibrations of Sections 6 and 7. We estimate $T_{\rm eff}$ using the $V-I_{\rm C}$ index, which has little intrinsic scatter above 2800 K (see Table 3 and Fig. 9). We then compute the bolometric correction in V band by linearly fitting the BC_V versus $V-I_{\rm C}$ relation (Fig. 8) in the colour range [1.95, 2.25]. As for the temperature calibration, this relation has little intrinsic scatter and the linear fit in the given range is accurate to 0.015 mag. Once the bolometric correction and the effective temperature are

Downloaded from http://mnras.oxfordjournals.org/ by guest on January 20, 2015

Table 3. Coefficients and range of applicability of our colour–temperature relations (equation 6). The photometric systems are $V(RI)_C$ for Johnson–Cousins, JHK_S for 2MASS, $(JK)_{DENIS}$ for DENIS and $(JHK)_{SAAO}$ for SAAO. For some indices, we caution the users from extrapolating these relations to redder colours than those given, as explained in Section 7.

Colour	Colour range	a_0	a_1	a_2	a_3	N	$\sigma(T_{\rm eff})$
$V-R_C$	[0.800, 2.310]	−1.4095	5.1212	−2.7937	0.5432	325	33
$V-I_C$	[1.400, 4.650]	0.5050	0.5562	−0.0593	0.0027	333	26
$V-J$	[2.260, 7.231]	0.1926	0.5738	−0.0726	0.0042	318	17
$V-H$	[2.946, 8.041]	−0.4711	0.8450	−0.1161	0.0066	315	23
$V-K_S$	[3.219, 8.468]	−0.4809	0.8009	−0.1039	0.0056	313	19
$V-J_{DENIS}$	[2.211, 7.124]	−0.0386	0.7709	−0.1243	0.0085	187	38
$V-K_{DENIS}$	[2.951, 8.306]	−0.2756	0.6907	−0.0846	0.0045	192	42
$V-J_{SAAO}$	[2.195, 4.115]	0.4445	0.3837	−0.0232	–	80	29
$V-H_{SAAO}$	[2.882, 4.802]	0.0406	0.4752	−0.0298	–	80	36
$V-K_{SAAO}$	[2.994, 5.063]	0.1609	0.3978	−0.0210	–	80	32
$(R-I)_C$	[0.660, 2.270]	0.8326	0.6122	−0.0849	0.0164	331	27
R_C-J	[1.503, 5.374]	0.3594	0.7223	−0.1401	0.0134	329	19
R_C-H	[2.053, 6.001]	−0.1645	0.9269	−0.1674	0.0135	332	31
R_C-K_S	[2.212, 6.428]	−0.0570	0.7737	−0.1226	0.0091	326	25
R_C-J_{DENIS}	[1.481, 5.214]	0.1541	0.9537	−0.2183	0.0215	165	41
R_C-K_{DENIS}	[2.221, 6.396]	−0.2094	0.8900	−0.1495	0.0109	160	43
R_C-J_{SAAO}	[1.434, 2.949]	0.6269	0.4385	−0.0334	–	81	32
R_C-H_{SAAO}	[2.121, 3.638]	0.1666	0.5733	−0.0466	–	81	41
R_C-K_{SAAO}	[2.233, 3.899]	0.2913	0.4615	−0.0299	–	81	35
I_C-J	[0.865, 2.954]	−0.3813	2.6488	−1.1642	0.1981	329	37
I_C-H	[1.433, 3.644]	−2.5844	4.3925	−1.5386	0.1941	338	77
I_C-K_S	[1.592, 4.085]	−1.8798	3.0706	−0.9024	0.0989	339	61
I_C-J_{SAAO}	[0.796, 1.428]	0.1346	1.6307	−0.4078	–	81	45
I_C-H_{SAAO}	[1.483, 2.118]	−1.6423	2.6765	−0.5318	–	81	85
I_C-K_{SAAO}	[1.595, 2.379]	−0.8748	1.6962	−0.2678	–	81	61

Notes. N is the number of stars employed for the fit after the 3σ clipping and $\sigma(T_{\rm eff})$ is the final standard deviation (in K) of the proposed calibrations.

Table 4. Comparison between the MOITE effective temperatures and angular diameters (columns 8 and 9) and the interferometric measured ones (columns 10 and 11).

Name	V	$U-B$	$B-V$	$V-R_C$	$V-I_C$	Ref.	$T_{\rm eff}$ (K)	$\theta_{\rm MOITE}$	$T_{\rm eff}$ (K)	$\theta_{\rm LD}$	Ref.
GJ 191	8.841	1.186	1.570	0.956	1.951	1	3661 ± 77	0.637 ± 0.028	3570 ± 156	0.692 ± 0.060	s
GJ 205†	7.968	1.183	1.475	0.972	2.055	2	3546 ± 106	1.093 ± 0.066	3520 ± 170	1.149 ± 0.110	s
GJ 411†	7.47	1.14	1.51	1.01	2.15	3	3467 ± 104	1.515 ± 0.091	3570 ± 42	1.436 ± 0.030	s
GJ 514	9.05	–	1.52	0.98	2.04	4	3594 ± 101	0.636 ± 0.037	3243 ± 160	0.753 ± 0.052	b
GJ 526†	8.464	–	–	0.971	2.070	5	3533 ± 106	0.884 ± 0.053	3636 ± 163	0.845 ± 0.057	b
GJ 699	9.553	1.264	1.737	1.228	2.779	6	3145 ± 69	1.003 ± 0.046	3163 ± 65	1.004 ± 0.040	s
GJ 752 A	9.115	1.138	1.515	1.039	2.333	2	3343 ± 107	0.835 ± 0.054	3368 ± 137	0.836 ± 0.051	b
GJ 880	8.65	–	1.497	0.985	2.103	4	3544 ± 153	0.822 ± 0.072	3277 ± 93	0.934 ± 0.059	b
GJ 887†	7.335	–	1.500	0.975	2.02	4	3577 ± 107	1.411 ± 0.085	3626 ± 56	1.388 ± 0.040	s

Source of the optical photometry: 1 – Kilkenny et al. (1998); 2 – Koen et al. (2002); 3 – Celis (1986); 4 – Bessell (1990a); 5 – The, Steenman & Alcaino (1984); 6 – Landolt (1983). In the IR we have used 2MASS JHK_S photometry (not reported here). † indicates a poor 2MASS photometry, so that the angular diameter has been obtained from the calibration of Sections 7 and 6 and not running the MOITE directly. Source of interferometric measurements: s – Ségransan et al. (2003); b – Berger et al. (2006).

known, the angular diameter can be readily computed (equation 14 in Casagrande et al. 2006). To these stars, we assign a 3 per cent error in $T_{\rm eff}$ and 6 per cent error in angular diameter, consistently with the errors obtained for the other stars in the sample. Although for these stars we are not applying the MOITE directly, we are using the calibrations obtained with the MOITE itself so that they are fully representative of our temperature and luminosity scale.

The overall comparison between our and the interferometric angular diameters shown in Fig. 10 is very good. Ségransan et al. (2003) and Berger et al. (2006) also compute effective temperatures which are obtained combining the measured $\theta_{\rm LD}$ with bolometric correction polynomial fit or comparing observed and model-predicted fluxes based on the observed angular diameters. This allows a direct comparison with their effective temperatures in Fig. 11 (filled diamonds). Only two stars deviate by more than 1σ from the one-to-one relation in Figs 10 and 11, namely GJ 514 and GJ 880. For these two stars, however, the two methods of determining $T_{\rm eff}$ from $\theta_{\rm LD}$ (i.e. using bolometric correction or comparing observed and model-predicted fluxes) return results discordant by 100 K. Choosing $T_{\rm eff}$ computed using bolometric correction (table 4 in Berger et al. 2006) would reduce by 100 K the discrepancy for these two stars in Fig. 11. We do not know the reason for such disagreement, however, our bolometric corrections are carefully determined from multiband data, whereas the main point of

Downloaded from http://mnras.oxfordjournals.org/ by guest on January 20, 2015

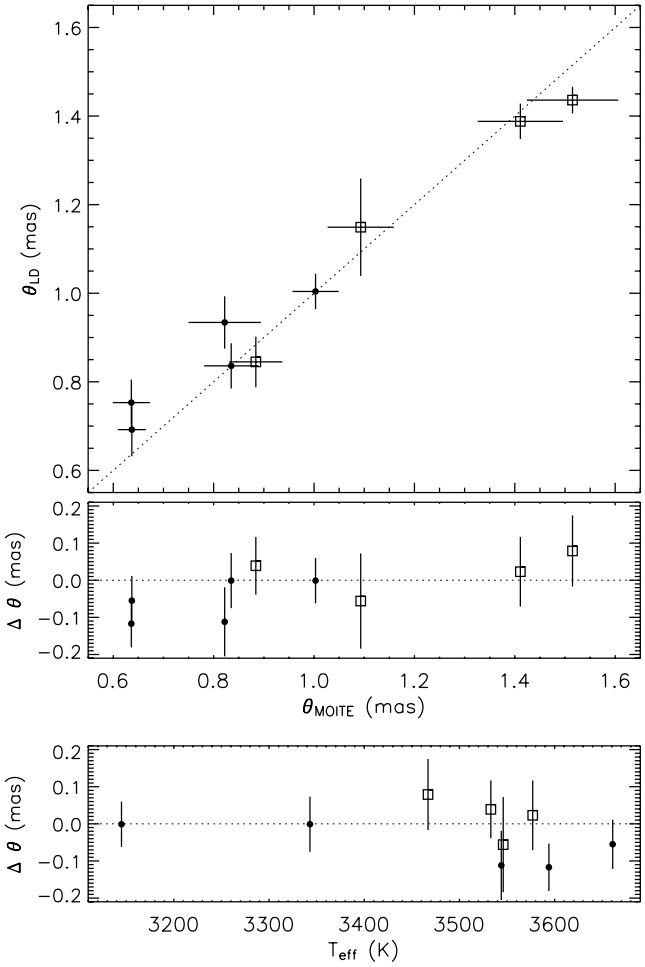

Figure 10. Comparison between our and the interferometric θ_{LD} angular diameters. Circles refer to angular diameters obtained applying the MOITE directly. Squares are for those stars for which the angular diameters have been computed from the colour–temperature and colour–luminosity calibrations of Sections 7 and 6. Dotted lines are intended to guide the eye.

interferometric studies is to precisely measure angular diameters (with which we are in good agreement), rather than determining accurate empirical bolometric corrections. The important point from the comparison in this section is that overall our angular diameters and effective temperatures agree with the trend defined by interferometric studies.

In particular, Barnard's star (GJ 699) is one of the benchmarks in setting the cool star temperature scale. Our angular diameter is in excellent agreement with the interferometric one and our effective temperature $T_{\rm eff} = 3145 \pm 69$ also closely matches the value of 3134 ± 102, obtained by the careful analysis of Dawson & De Robertis (2004).

7.2 Comparison with other temperature scales

The determination of effective temperatures by means of different techniques below 4000 K becomes increasingly difficult as a result of the increasing complexity of the stellar spectra and previous studies have usually computed $T_{\rm eff}$ for a limited number of stars. Interferometry has recently provided a breakthrough to anchor the temperature scale down to 3000 K, as discussed in Section 7.1. Moreover, stars cooler than 3000 K have angular diameters too

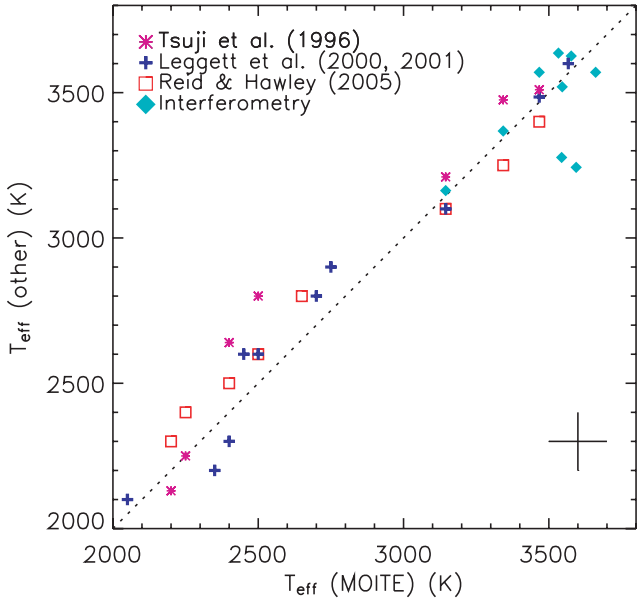

Figure 11. Comparison between the MOITE effective temperatures and those determined in other recent studies. A typical error bar of ±100 K is shown in the lower right-hand corner. Dotted line with slope 1 is intended to guide the eye.

small to be resolved by currently available interferometers. Here we compare our effective temperatures to those obtained by various recent studies.

Among the possible different techniques to estimate $T_{\rm eff}$, one is to fit observed molecular features with model predictions (e.g. Kirkpatrick et al. 1993). However, these features might depend not only on the effective temperature, but also on other effects of line formation and the reliability of the models themselves. It is a long-standing result that especially below 3500–3000 K such a technique returns effective temperatures that are higher by several hundred Kelvin with respect to other more empirically motivated methods (e.g. Pavlenko & Jones 2002; Jones et al. 2005). Very recently, Viti et al. (2008) have proposed a new and promising technique based on very high resolution mid-IR observations of pure rotational water vapour transitions in M dwarfs. Another approach is to compare observed and synthetic spectra and estimate $T_{\rm eff}$ from the model that better matches the observation in the IR (e.g. Leggett et al. 2000, 2001), in the optical (e.g. Dawson & De Robertis 2000) or throughout most of the spectrum (e.g. Pavlenko et al. 2006). Burgasser & Kirkpatrick (2006) have shown that the parameters derived using optical or near-IR fits for a given object exhibit clear systematic differences up to 100–200 K in effective temperature and 0.5–1.0 dex in metallicity.

A more consistent way to determine $T_{\rm eff}$ is to analyse the entire spectral region contributing to the bolometric flux, although in the past this approach has been done mostly with blackbody calibrations rather than with model predictions (e.g. Veeder 1974; Reid & Gilmore 1984). A more rigorous attempt to recover the bolometric flux was used by Tsuji et al. (1996). Finally, Reid & Hawley (2005) have collected spectroscopic and photometric $T_{\rm eff}$ estimates of a few well studied nearby M dwarfs covering the spectral-type M0 to M9 (their table 4.1).

We have searched in the literature for other $T_{\rm eff}$ determination of our stars and did not find many, particularly below 3000 K. To increase the number of stars available for the comparison, we have applied our technique to a few more very red dwarfs (LHS 36, LHS 68,

Downloaded from http://mnras.oxfordjournals.org/ by guest on January 20, 2015

LHS 292, LHS 429, LHS 2065, LHS 2924, LHS 3003) which are commonly studied in the literature. For these stars optical colours are available from Bessell (1990a, 1991) and IR from 2MASS. We caution that they are all classified as flare stars in SIMBAD and for this reason they were not included in the original sample of Section 2. The effective temperatures for these and few other cool stars from Tables 1, 2 and 4 are discussed below.

LHS 2 – (GJ 1002). For this star we obtain $T_{\rm eff} = 2750$ K, slightly cooler than the temperature of 2900 K obtained by Leggett et al. (2000).

LHS 36 – (GJ 406). We obtain an effective temperature of 2500 K which is cooler by about 100 K than the value of 2600 K obtained by Leggett et al. (2000) and reported also in Reid & Hawley (2005). For the same star Pavlenko et al. (2006) obtained an effective temperature of 2800 K after a critical examination of the most recent model atmosphere fit to this object. The same temperature was also obtained by Tsuji et al. (1996). Golimowski et al. (2004) also found a hotter temperature than we do (2900 K).

LHS 37 – (GJ 411). For this star we obtain $T_{\rm eff} = 3467$ K which is in agreement with 3510 K reported in Tsuji et al. (1996), 3500 K in Leggett et al. (1996) and 3400 K in Reid & Hawley (2005).

LHS 39 – (GJ 412 B). We obtain an effective temperature of 2700 K, which again is cooler by 100 K with respect to the value obtained by Leggett et al. (2000) (2800 K).

LHS 57 – (GJ 699). Our value $T_{\rm eff} = 3145$ K is halfway between 3100 K in Leggett et al. (2000), Reid & Hawley (2005) and 3210 K in Tsuji et al. (1996).

LHS 65 – (GJ 821). For this *Hipparcos* star we obtain $T_{\rm eff} = 3567$ K, in close agreement with 3600 K in Leggett et al. (2000).

LHS 68 – (GJ 866). This dwarf, together with GJ 406, is one of the reddest standards of the $BV(RI)_{\rm C}$ system. Unfortunately, it is member of a triple system, which might decrease the accuracy of the photometry (Delfosse et al. 1999). We obtain $T_{\rm eff} = 2650$ K, considerably cooler than the value of 3000 K obtained by Dawson & De Robertis (2000) but in better agreement with $T_{\rm eff} = 2800$ K in Reid & Hawley (2005).

LHS 292 – (GJ 3622). Our technique returns $T_{\rm eff} = 2450$ K, cooler then both Leggett et al. (2000) (2600 K) and Golimowski et al. (2004) (2725 K).

LHS 429 – (GJ 644 C). The MOITE returns $T_{\rm eff} = 2400$ K for this late M dwarf, which is now 100 K hotter than in Leggett et al. (2000) but cooler than the value of 2500 K in Reid & Hawley (2005) and 2640 K in Tsuji et al. (1996).

LHS 473 – (GJ 752 A). The effective temperature we obtain 3343 K is mid-way between 3250 K in Reid & Hawley (2005) and 3475 K in Tsuji et al. (1996).

LHS 474 – (GJ 752 B). We obtain $T_{\rm eff} = 2250$ K which compares nicely with Tsuji et al. (1996) (2250 K) but it is slightly cooler than 2400 K in Reid & Hawley (2005).

LHS 2065 – (GJ 3517). For this very red dwarf we obtain $T_{\rm eff} = 2050$ K in rough agreement with Leggett et al. (2001) (2100 K) but much cooler than the temperature of 2400 K obtained by Golimowski et al. (2004).

LHS 2924 – (GJ 3849). According to Reid & Hawley (2005) this is the best-studied M9 dwarf for which they report $T_{\rm eff} = 2300$ K. We obtain an effective temperature of 2200 K which is slightly hotter than the value of 2130 K in Tsuji et al. (1996).

LHS 3003 – (GJ 3877). We obtain $T_{\rm eff} = 2350$ K which is now hotter than Leggett et al. (2001) (2200 K), but still cooler than Golimowski et al. (2004) (2600 K).

Our temperatures are shown in Fig. 11 against other studies discussed here or in Section 7.1. There is an overall good agreement with respect to the effective temperatures obtained by Leggett et al. (2000, 2001), especially above 3000 K. Below this temperature typical differences of order 100 K exist, but on average the scatter in the data suggest we are on the same scale. Similarly, we are in very good agreement with the temperatures reported in Reid & Hawley (2005) above 3000 K, whereas below this temperature we are systematically cooler by 100 K. We also agree within 100 K with Tsuji et al. (1996) except for effective temperatures around 2500 K where we have two stars with larger differences. Our effective temperatures are also 250–400 K cooler than those in Golimowski et al. (2004) which are estimated using the relationship between the bolometric luminosity (their observable) and $T_{\rm eff}$ predicted from evolutionary models.

Summarizing, further work is needed before reaching a consensus among different temperature scales, especially below 3000 K. However, our temperatures are supported from interferometric angular diameters between 3100 and 3600 K and the homogeneous and smooth colour–temperature relations of Fig. 9 lead us to believe our temperature scale is credible below 3000 K. Furthermore, the data in Fig. 11 suggest that despite case-by-case differences, on average we agree with the effective temperature reported in many recent studies.

8 ON THE DISCONTINUOUS TRANSITION FROM K TO M DWARFS

In our previous paper we have implemented the IRFM to derive effective temperatures and bolometric luminosities of G and K dwarfs. Here we have extended our technique to much cooler effective temperatures. For M dwarfs with accurate *Hipparcos* parallaxes (i.e. those from Koen et al. 2002) we can compute absolute magnitudes and therefore plot them with our previous sample from Casagrande et al. (2006) and study the properties of the entire lower main sequence (Fig. 12), finding a very interesting feature: whereas the transition from late K to early M type occurs smoothly in the widely used $M_V - (B - V)$ plane, in IR colours (which are better tracers of $M_{\rm Bol}$ and $T_{\rm eff}$) a prominent discontinuity appears around late K to early M types. The discontinuity is clearly evident in the observational plane $M_{K_{\rm S}} - (V - K_{\rm S})$ (and we have verified it is present also in the other IR colours) and is also quite prominent in the theoretical $M_{\rm Bol} - T_{\rm eff}$ plane, at around 4200–4300 K (Fig. 12).

The feature is close to the point at which our two calibrations (IRFM for G and K dwarfs and MOITE for M dwarfs) meet. To confirm the discontinuity is not dependent on the calibrations, we have reprocessed all the stars in Casagrande et al. (2006) with the MOITE, and using the Phoenix model atmosphere, confirming that we obtain the same temperatures and luminosities with both methods above ∼4000 K.

For both the GK dwarfs in Casagrande et al. (2006) and the M dwarfs studied here we have used strict selection criteria to remove double and variable stars. For the sake of completeness, we note that when the M dwarfs labelled as variable in Koen et al. (2002) are plotted in both the observational and $M_{\rm Bol} - T_{\rm eff}$ planes of the HR diagram, these follow the same trend defined from the *Hipparcos* stars of Section 2.

We note that the discontinuity is as clear in the purely observational plane most sensitive to temperature and luminosity $[M_{K_{\rm S}} - (V - K_{\rm S})]$ as it is in the $M_{\rm Bol}$–$T_{\rm eff}$ plane: we thus consider the temperature–luminosity discontinuity to be real. It occurs at 4200–4300 K, appearing as a plateau in the temperature–luminosity plane, with the luminosity of the M dwarfs holding fairly steady even as their temperatures decrease. For this to occur, the radii of the M

Downloaded from http://mnras.oxfordjournals.org/ by guest on January 20, 2015

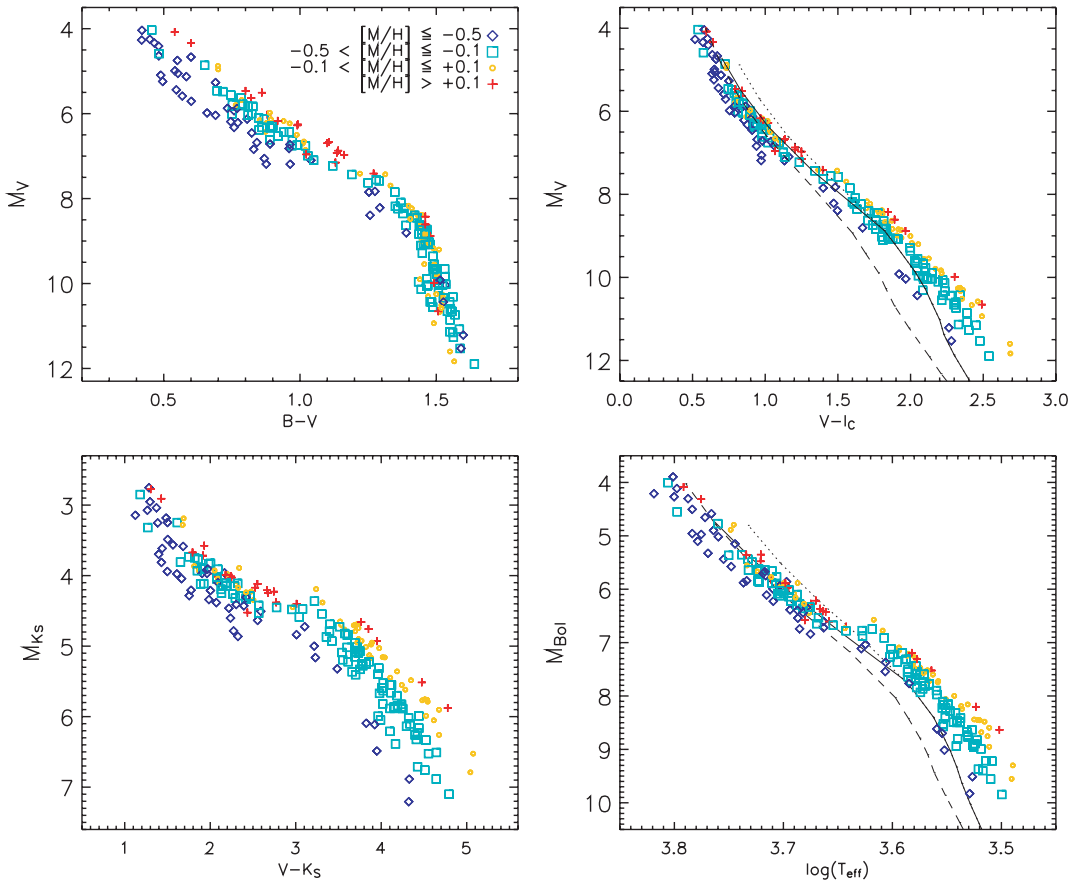

Figure 12. HR diagram in different planes. Only stars with *Hipparcos* parallaxes better than 15 per cent are used. Overplotted are also the theoretical isochrones from Baraffe et al. (1998) for [M/H] = 0.0 (dotted) and [M/H] = −0.5 (dashed) for $\alpha_{\rm MLT} = 1$. The continuous line is a solar calibrated model with $\alpha_{\rm MLT} = 1.9$. For all the isochrones the age used is 5 Gyr. In the last panel both our sample of stars and the theoretical isochrones have been plotted adopting $M_{\rm Bol,\odot} = 4.74$. Notice that the metallicities for the stars plotted here are either from high-resolution spectroscopy (Casagrande et al. 2006) or from the Bonfils et al. (2005) calibration.

dwarfs must be increasing again, rather than falling monotonically going down the main sequence.

In Fig. 12, we compare our stars with the very low mass star evolutionary models of Baraffe et al. (1998). We have adopted 5-Gyr-old isochrones, although the evolution of the lower main sequence is practically insensitive to the age for $M_{\rm Bol} > 5.4$ (e.g. Casagrande et al. 2007). Fig. 12 shows that these models do not appear to reproduce the discontinuity in the main sequence at 4200–4300 K.

For further insight in the problem, in Fig. 13 the observed radius–luminosity, radius–mass and the mass–luminosity relations are compared with the theoretical prediction from the same Baraffe et al. (1998) models. We have estimated the masses of our stars

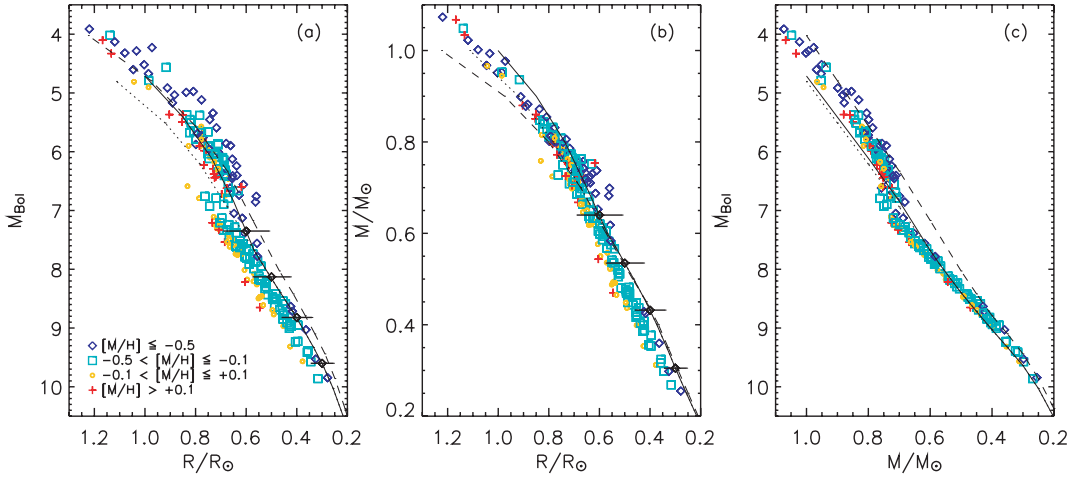

Figure 13. Comparison with the Baraffe et al. (1998) models as in Fig. 12 but for the (a) radius–luminosity, (b) radius–mass and (c) mass–luminosity relations. Error bars of ±15 per cent in radius are shown for 0.6, 0.5, 0.4, 0.3 $R_\odot$ for the solar metallicity model.

© 2008 The Authors. Journal compilation © 2008 RAS, MNRAS **389,** 585–607

Downloaded from http://mnras.oxfordjournals.org/ by guest on January 20, 2015

using the empirical *K*-band mass–luminosity calibration of Delfosse et al. (2000) which applies for $M_K \geq 4.5$. For brighter luminosities we have used the empirical relation in *K* band from Henry & McCarthy (1993). The use of two different calibrations – which are however fully consistent – might be responsible for same small offset, but the overall trend is well defined. We also convert our 2MASS photometry into the CIT (California Institute of Technology) system (Carpenter 2001) before applying the aforementioned empirical calibrations. In Figs 13(a) and (b) it is obvious that current models underestimate the radii of the M dwarfs by 15–20 per cent, as already noticed by several other authors (see Ribas 2006, for a review). Such a definite conclusion has been obtained using double-lined eclipsing binaries. Our study reinforces the finding and confirms its existence also to single field stars (Berger et al. 2006). For the mass–luminosity relation in Fig. 13(c), the disagreement between data and theoretical models is less dramatic. In particular, going to masses below $0.5\,M_{\odot}$ the agreement improve considerably as already noticed by other authors (e.g. Delfosse et al. 2000). Since such a good agreement between the data and the models is neither present in the other panels of Fig. 13 nor in the temperature–luminosity plane of Fig. 12, it argues in favour of a scenario in which the stars have larger radii and cooler effective temperatures than predicted by models, but just in right proportion to barely affect the luminosities.

In what follows we briefly discuss possible mechanisms responsible for the radius increase which marks the transition from K to M dwarfs. An interesting discussion on the disagreement between the predicted and measured radii of very low mass stars from eclipsing binaries and interferometry can be found e.g. in López-Morales (2007). We also mention that another discontinuity at cooler effective temperatures ($V - I_C \sim 2.7$), i.e. when the M dwarfs become fully convective, is already known in literature (e.g. Hawley et al. 1996; Clemens et al. 1998; Koen et al. 2002) and we do not discuss it here.

8.1 Mixing length

Very low mass stars are a very interesting place to test the input physics in stellar models, since below $\sim 0.4\,M_{\odot}$ (depending on the metallicity and the inclusion of magnetic fields in the models) stellar interiors are expected to become fully convective. Their evolution is thus practically insensitive to the mixing length parameters $\alpha_{\rm MLT}$ and the models thus are not subject to any adjustable parameter other than the helium abundance (which is expected to be solar scaled). For this reason, very low mass models do not need to be calibrated on the Sun.

The Baraffe et al. (1998) models are computed assuming a mixing length $\alpha_{\rm MLT} = 1$, quite different to values of 1.5–2 which are typically adopted for the Sun, and it is this which leads to the difference between the models and data for the G and K dwarfs in Fig. 12. In fact, if a solar calibrated model is used (Baraffe et al. 1998, continuous line), the agreement for those stars becomes excellent. We have already extensively tested theoretical models for G and K dwarfs in our previous paper (Casagrande et al. 2007) and so we focus here on the M dwarfs.

A possible solution to the discontinuity in the HR diagram could be a rapid decrease of the mixing length as a function of stellar mass, although this would keep rather unaffected the lower part of the HR diagram in Fig. 12, where theoretical isochrones would still remain offset with respect to the observed stars. Since the mixing length describes the efficiency of the convection, any physical mechanism inhibiting convection (like magnetic activity discussed in Section 8.2) can be phenomenologically mimicked by decreasing the mixing length (Chabrier, Gallardo & Baraffe 2007). Very interestingly, there are indications of a possible dependence of the mixing length with mass from modelling the components of binaries (e.g. Lebreton, Fernandes & Lejeune 2001; Yildiz et al. 2006). Just how viable this solution is we regard as an open question.

8.2 Magnetic activity

The discrepancy between the predicted and observed radii in M dwarfs could be related to the activity level of the stars (e.g. Torres & Ribas 2002; López-Morales & Ribas 2005; Morales, Ribas & Jordi 2008). It is known that active and inactive M dwarfs define two different sequences in the luminosity–colour (Stauffer & Hartmann 1986) and temperature–radius (Mullan & MacDonald 2001) plane. Strong magnetic fields are expected to inhibit convection, thus giving larger radii for a given $T_{\rm eff}$ or lower $T_{\rm eff}$ for a given radius (Mullan & MacDonald 2001). Alternatively, it has also been suggested that the larger radii could simply be an effect of flux conservation in a magnetic spot-covered stellar surface (López-Morales & Ribas 2005).

The stars with *Hipparcos* parallaxes plotted in Fig. 12 are expected to have a very low activity level because of the strict selection criteria used in Section 2. This however does not exclude the possibility of a large and homogeneous spot coverage since that would not necessarily produce any strong variability. To gauge further insight into the problem, we have checked that when the stars labelled as variable in Koen et al. (2002) are included in Fig. 12, they define the same trend shown by the stars of Section 2. Notice though that the M dwarfs in Koen et al. (2002) were selected among the less variable in *Hipparcos*. Dedicated studies of active M dwarfs should still be done before reaching a more firm conclusion: at present, although magnetic activity can undoubtedly affect stellar radii, we regard it as unlikely as being responsible for the main-sequence discontinuity observed at 4200–4300 K. Concede the effect of magnetic field certainly becomes more important descending the main sequence and its inclusion is likely to be a relevant ingredient also for a proper modelling of non-active M dwarfs.

8.3 Opacity

The models clearly have difficulty in reproducing the strong transition between late K- and early M-type dwarfs, but the disagreement becomes even more pronounced as one descends to the bottom of the main sequence. Similar disagreement was already noticed by Baraffe et al. (1998) when comparing their models with a sample of field stars, open and globular clusters with metallicities similar to those covered in the present study. Since the disagreement is much less pronounced in the comparison with metal-poor globular cluster M dwarfs (Baraffe et al. 1997), the disagreement at high metallicity might be ascribed to missing opacity of some sort in the models.

Figs 12 and 13 also indicate that the disagreement is more marked for metal-rich stars, again suggesting that missing opacity sources could be a viable solution (Berger et al. 2006). It is very interesting that the discontinuity occurs at a temperature when molecular formation (H_2O and TiO) starts to be important, again suggesting that opacity is a possible culprit.

8.4 Three characters in search of an author

We have briefly discussed three possible causes for the luminosity–temperature discontinuity in the main sequence going from K to

Downloaded from http://mnras.oxfordjournals.org/ by guest on January 20, 2015

M dwarfs. The data in Figs 12 and 13 suggest that the problem is more likely to be related to molecular opacity, than being structural, but considerable further work is needed to test those ideas. Simple steps forward to confirm or rule out possible explanations would be the analysis of late K and early M dwarfs' spectra as well as to run the MOITE for a large sample of (magnetically) active M dwarfs, to help in searching for correlation between the radius discrepancy and activity level or other physical parameters (e.g. López-Morales 2007). Of course, there may be no a unique culprit for the radius discontinuity in M dwarfs, and only advances in modelling both the structure and the atmosphere of these stars will get things right.

9 CONCLUSIONS

We have determined the temperature scale of M dwarfs, using stars with very accurate multiband photometry from optical to near-IR and the MOITE, a new method which exploits the flux ratio in different bands as a sensitive indicator of both effective temperatures and metallicities. Our proposed temperature scale extends down to $T_{\rm eff} \sim$ 2100–2200 K, i.e. to the L dwarf limit (e.g. Leggett et al. 2002), and above ∼3000 K is supported from interferometric angular diameters. Our metallicities, which are ultimately calibrated on Bonfils et al. (2005) metallicity scale, are also found to be in very good agreement with the latest measurements from Woolf & Wallerstein (2005, 2006) and Bean et al. (2006a,b), even if significant differences in the various effective temperature scales still exist. Cool M dwarfs with metallicities based on (hotter) *Hipparcos* common proper motion companions also suggest our metallicities are reliable even below 3000 K, although further data are needed. Accurate multiband photometry for the coolest *Hipparcos* common proper-motion pairs would permit one to firmly extend the MOITE to the bottom of the main sequence, thus opening this elusive area also to galactic chemical evolution investigations. Exoplanets are found around M dwarfs, and a uniform metallicity scale for their host stars will also be very useful.

The high quality of our data allows us to identify a striking feature which marks the transition from K to M dwarfs, which appears to be due to an increase in the radii of the early M dwarfs relative to late K dwarfs. We have compared our sample of stars with theoretical isochrones for low-mass stars and find that such a feature is not predicted by the models, substantially confirming the disagreement already noticed in the case of eclipsing binaries. Possible explanations including the effect of magnetic fields and molecular opacity have been discussed.

This work also highlights the potentiality of high accuracy multiband photometry in determining fundamental stellar parameters and identifying fine details in the HR diagram. In particular, the MOITE will hugely benefit from the existing IR (2MASS, DENIS) and forthcoming optical surveys like SkyMapper (Keller et al. 2007), Pan-Starrs (Kaiser et al. 2002) and Large Synoptic Survey Telescope (LSST; Claver et al. 2004) which will provide accurate and homogeneous multicolour and multi-epoch photometry for a large number of stars.

ACKNOWLEDGMENTS

LC acknowledges the Turku University Foundation and the Otto A. Malm Foundation for financial support. This study was also funded by the Academy of Finland (CF). We are indebted to C. Koen for providing the SAAO photometry and a careful reading on the first draft of the paper. We thank the Phoenix team for making their models publicly available and P. Hauschildt and I. Brott for useful correspondence as well as M. Asplund for the same kindness. L. Portinari is also acknowledged for enlightening discussions. We are also indebted to B. Gustafsson for relevant comments and insight on many points of the paper. We thank an anonymous referee for many useful comments and suggestions which have significantly improved the presentation of the paper. The research has made use of the General Catalogue of Photometric Data operated at the University of Lausanne and the SIMBAD data base, operated at CDS, Strasbourg, France. The publication makes use of the data products from the 2MASS, which is a join project of the University of Massachusetts and the Infrared Processing and Analysis Centre/California Institute of Technology, funded by the National Aeronautics and Space Administration and the National Science Foundation.

REFERENCES

Allard F., 1990, PhD thesis, Univ. Heidelberg
Allard F., Hauschildt P. H., 1995, ApJ, 445, 433
Allard F., Hauschildt P. H., Alexander D. R., Starrfield S., 1997, ARA&A, 35, 137
Allende Prieto C., Asplund M., López R. J. G., Lambert D. L., 2002, ApJ, 567, 544
Allred J. C., Hawley S. L., Abbett W. P., Carlsson M., 2006, ApJ, 644, 484
Auman J. R. J., 1969, ApJ, 157, 799
Baraffe I., Chabrier G., Allard F., Hauschildt P. H., 1997, A&A, 327, 1054
Baraffe I., Chabrier G., Allard F., Hauschildt P. H., 1998, A&A, 337, 403
Bean J. L., Sneden C., Hauschildt P. H., Johns-Krull C. M., Benedict G. F., 2006a, ApJ, 652, 1604
Bean J. L., Benedict G. F., Endl M., 2006b, ApJ, 653, 65
Berger D. H. et al., 2006, ApJ, 644, 475
Bessell M. S., 1986, PASP, 98, 354
Bessell M. S., 1990a, A&AS, 83, 357
Bessell M. S., 1990b, PASP, 102, 1181
Bessell M. S., 1991, AJ, 101, 662
Bessell M. S., Castelli F., Plez B., 1998, A&A, 333, 231
Bigot L., Kervella P., Thévenin F., Ségransan D., 2006, A&A, 446, 635
Blackwell D. E., Shallis M. J., 1977, MNRAS, 180, 177
Blackwell D. E., Shallis M. J., Selby M. J., 1979, MNRAS, 188, 847
Blackwell D. E., Petford A. D., Shallis M. J., 1980, A&A, 82, 249
Bochanski J. J., Hawley S. L., Reid I. N., Covey K. R., West A. A., Tinney C. G., Gizis J. E., 2005, AJ, 130, 1871
Bochanski J. J., Munn J. A., Hawley S. L., West A. A., Covey K. R., Schneider D. P., 2007, AJ, 134, 2418
Bohlin R. C., 2007, in Sterken C., ed., ASP Conf. Ser. Vol. 364, The Future of Photometric, Spectrophotometric and Polarimetric Standardization. Astron. Soc. Pac., San Francisco, p. 315
Bohlin R. C., Gilliland R. L., 2004, AJ, 127, 3508
Bonfils X., Delfosse X., Udry S., Santos N. C., Forveille T., Ségransan D., 2005, A&A, 442, 635
Bonfils X. et al., 2007, A&A, 474, 293
Brett J. M., 1995a, A&AS, 109, 263
Brett J. M., 1995b, A&A, 295, 736
Brett J. M., Plez B., 1993, Proc. Astron. Soc. Aust., 10, 250
Brott I., Hauschildt P. H., 2005, in Turon C., O'Flaherty K. S., Perryman M. A. C., eds, ESA SP-576, The Three-Dimensional Universe with Gaia: A PHOENIX Model Atmosphere Grid for Gaia. ESA, Noordwijk, p. 565
Burgasser A. J., Kirkpatrick J. D., 2006, ApJ, 645, 1485
Burgasser A. J., Cruz K. L., Kirkpatrick J. D., 2007, ApJ, 657, 494
Burrows A., Hubbard W. B., Saumon D., Lunine J. I., 1993, ApJ, 406, 158
Butler R. P., Vogt S. S., Marcy G. W., Fischer D. A., Wright J. T., Henry G. W., Laughlin G., Lissauer J. J., 2004, ApJ, 617, 580
Carpenter J. M., 2001, AJ, 121, 2851
Carter B. S., 1990, MNRAS, 242, 1
Carter B. S., Meadows V. S., 1995, MNRAS, 276, 734
Casagrande L., Portinari L., Flynn C., 2006, MNRAS, 373, 13

Downloaded from http://mnras.oxfordjournals.org/ by guest on January 20, 2015

Casagrande L., Flynn C., Portinari L., Girardi L., Jimenez R., 2007, MNRAS, 382, 1516
Castelli F., Kurucz R. L., 2003, in Piskunov N., Weiss W. W., Gray D. F., eds, Proc. IAU Symp. 210, Modelling of Stellar Atmospheres. Astron. Soc. Pac., San Francisco, p. A20
Celis S. L., 1986, ApJS, 60, 879
Chabrier G., Gallardo J., Baraffe I., 2007, A&A, 472, 17
Claret A., 2000, A&A, 363, 1081
Claver C. F. et al., 2004, SPIE, 5489, 705
Clemens J. C., Reid I. N., Gizis J. E., O'Brien M. S., 1998, ApJ, 496, 352
Cohen M., Walker R. G., Barlow M. J., Deacon J. R., 1992, AJ, 104, 1650
Cohen M., Wheaton Wm. A., Megeath S. T., 2003, AJ, 126, 1090
Davis J., Tango W. J., 1986, Nat, 323, 234
Dawson P. C., De Robertis M. M., 2000, AJ, 120, 1532
Dawson P. C., De Robertis M. M., 2004, AJ, 127, 2909
Delfosse X., Forveille T., Mayor M., Perrier C., Naef D., Queloz D., 1998, A&A, 338, 67
Delfosse X., Forveille T., Udry S., Beuzit J.-L., Mayor M., Perrier C., 1999, A&A, 350, 39
Delfosse X., Forveille T., Ségransan D., Beuzit J. L., Udry S., Perrier C., Mayor M., 2000, A&A, 364, 217
Dommanget J., Nys O., 1994, Commun. Obs. R. Belg. Ser. A, 115, 1
Gizis J. E., Reid I. N., Hawley S. L., 2002, AJ, 123, 3356
Glass I. S., 1974, Mon. Notes Astron. Soc. South. Afr., 33, 53
Golimowski D. A. et al., 2004, AJ, 127, 3516
Gould A., Chanamé J., 2004, ApJS, 150, 455
Gould A., Bahcall J. N., Flynn C., 1997, ApJ, 482, 913
Gould A., Flynn C., Bahcall J. N., 1998, ApJ, 503, 798
Graham J. A., 1982, PASP, 94, 244
Gustafsson B., 1989, ARA&A, 27, 701
Habets G. M. H. J., Heintze J. R. W., 1981, A&AS, 46, 193
Hanbury Brown R., Davis J., Allen L. R., 1974, MNRAS, 167, 475
Hauschildt P. H., Allard F., Baron E., 1999a, ApJ, 512, 377
Hauschildt P. H., Allard F., Ferguson J., Baron E., Alexander D. R., 1999b, ApJ, 525, 871
Hauschildt P. H., Allard F., Baron E., Aufdenberg J., Schweitzer A., 2003, in Munari U., ed., ASP Conf. Ser. Vol. 298, GAIA Spectroscopy: Science and Technology. Astron. Soc. Pac., San Francisco, p. 179
Hawkins M. R. S., Bessell M. S., 1988, MNRAS, 234, 177
Hawley S. L., Gizis J. E., Reid I. N., 1996, AJ, 112, 2799
Henry T. J., McCarthy D. W. J., 1993, AJ, 106, 773
Henry T. J., Subasavage J. P., Brown M. A., Beaulieu T. D., Jao W. C., Hambly N. C., 2004, AJ, 128, 2460
Jones H. R. A., Pavlenko Ya., Viti S., Barber R. J., Yakovina L. A., Pinfield D., Tennyson J., 2005, MNRAS, 358, 105
Kaiser N. et al., 2002, SPIE, 4836, 154
Keller S. C. et al., 2007, Publ. Astron. Soc. Aust., 24, 1
Kerber L. O., Javiel S. C., Santiago B. X., 2001, A&A, 365, 424
Kervella P., Thévenin F., Morel P., Bordé P., Di Folco E., 2003, A&A, 408, 681
Kilkenny D., van Wyk F., Roberts G., Marang F., Cooper D., 1998, MNRAS, 294, 93
Kilkenny D., Koen C., van Wyk F., Marang F., Cooper D., 2007, MNRAS, 380, 1261
Kirkpatrick J. D., Kelly D. M., Rieke G. H., Liebert J., Allard F., Wehrse R., 1993, ApJ, 402, 643
Kirkpatrick J. D., McGraw J. T., Hess T. R., Liebert J., McCarthy D. W. J., 1994, ApJS, 94, 749
Koen C., Kilkenny D., van Wyk F., Cooper D., Marang F., 2002, MNRAS, 334, 20
Kron G. E., 1952, ApJ, 115, 301
Kui R., 1991, PhD thesis, National Univ. Australia
Lacy C. H., 1977, ApJ, 218, 444
Laing J. D., 1989, South Afr. Astron. Obs. Circ., 13, 29
Landolt A. U., 1983, AJ, 88, 439
Landolt A. U., 1992, AJ, 104, 340
Lane B. F., Boden A. F., Kulkarni S. R., 2001, ApJ, 551, 81
Lebreton Y., Fernandes J., Lejeune T., 2001, A&A, 374, 540
Leggett S. K., Allard F., Berriman G., Dahn C. C., Hauschildt P. H., 1996, ApJS, 104, 117
Leggett S. K., Allard F., Dahn C., Hauschildt P. H., Kerr T. H., Rayner J., 2000, ApJ, 535, 965
Leggett S. K., Allard F., Geballe T. R., Hauschildt P. H., Schweitzer A., 2001, ApJ, 548, 908
Leggett S. K. et al., 2002, ApJ, 564, 452
López-Morales M., 2007, ApJ, 660, 732
López-Morales M., Ribas I., 2005, ApJ, 631, 1120
Metcalfe T. S., Mathieu R. D., Latham D. W., Torres G., 1996, ApJ, 456, 356
Morales J. C., Ribas I., Jordi C., 2008, A&A, 478, 507
Mould J. R., 1975, A&A, 38, 283
Mould J. R., 1976, A&A, 48, 443
Mozurkewich D. et al., 2003, AJ, 126, 2502
Mullan D. J., MacDonald J., 2001, ApJ, 559, 353
Pavlenko Ya. V., Jones H. R. A., 2002, A&A, 396, 967
Pavlenko Ya. V., Jones H. R. A., Lyubchik Yu., Tennyson J., Pinfield D. J., 2006, A&A, 447, 709
Pirzkal N. et al., 2005, ApJ, 622, 319
Price S. D., Paxson C., Engelke C., Murdock T. L., 2004, AJ, 128, 889
Reid N., Gilmore G., 1984, MNRAS, 206, 19
Reid I. N., Hawley S. L., 2005, New Light on Dark Stars, 2nd edn. Springer, New York
Reid I. N., Gizis J. E., Cohen J. G., Pahre M. A., Hogg D. W., Cowie L., Hu E., Songaila A., 1997, PASP, 109, 559
Reid I. N., Burgasser A. J., Cruz K. L., Kirkpatrick J. D., Gizis J. E., 2001, AJ, 121, 1710
Reid I. N., Kilkenny D., Cruz K. L., 2002, AJ, 123, 2822
Reid I. N. et al., 2003, AJ, 126, 3007
Reid I. N. et al., 2004, AJ, 128, 463
Reiners A., Basri G., 2007, ApJ, 656, 1121
Ribas I., 2006, Ap&SS, 304, 89
Ségransan D., Kervella P., Forveille T., Queloz D., 2003, A&A, 397, 5
Stauffer J. R., Hartmann L. W., 1986, ApJS, 61, 531
The P. S., Steenman H. C., Alcaino G., 1984, A&A, 132, 385
Tinney C. G., Mould J. R., Reid I. N., 1993, AJ, 105, 1045
Tokunaga A. T., Vacca W. D., 2005, PASP, 117, 421
Torres G., Ribas I., 2002, ApJ, 567, 1140
Tsuji T., 1969, in Kumar S. S., ed., Low-Luminosity Stars. Gordon & Breach, New York, p. 457
Tsuji T., Ohnaka K., Aoki W., 1996, A&A, 305, 1
Udry S. et al., 2007, A&A, 469, 43
Veeder G. J., 1974, AJ, 79, 1056
Viti S., Jones H. R. A., Richter M. J., Barber M. J., Tennyson J., Lacy J. H., 2008, MNRAS, 388, 1305
West A., Bochanski J. J., Hawley S. L., Cruz K. L., Covey K. R., Silvestri N. M., Reid I. N., Liebert J., 2006, AJ, 132, 2507
Woolf V. M., Wallerstein G., 2005, MNRAS, 356, 963
Woolf V. M., Wallerstein G., 2006, PASP, 118, 218
Yildiz M., Yakut K., Bakiş H., Noels A., 2006, MNRAS, 368, 1941
Zheng Z., Flynn C., Gould A., Bahcall J. N., Salim S., 2001, ApJ, 555, 393
Zheng Z., Flynn C., Gould A., Bahcall J. N., Salim S., 2004, ApJ, 601, 500

APPENDIX A: MOITE, TECHNICAL DETAILS

We use the Phoenix grid of synthetic spectra presented in Section 3 to bootstrap the MOITE. We assume $\log(g) = 5.0$ throughout but we have tested that a change of ± 0.5 dex in the assumed surface gravity has negligible effect on the results.

For any given star in our sample, we first use the $T_{\rm eff} : (R - I)_{\rm C}$ calibration of Bessell (1991) to obtain an initial estimate of the effective temperature $T_{\rm eff,0}$. We then interpolate over our grid of Phoenix model atmosphere to compute the flux missing from our multiband photometry and reconstruct the bolometric flux on the Earth. At each n iteration a new $T_{{\rm eff},n}$ is obtained – according to

Downloaded from http://mnras.oxfordjournals.org/ by guest on January 20, 2015

equation (1) or equation (3) – until $|T_{\rm eff,\it n} - T_{\rm eff,\it n-1}| < 1$ K and the final solution is thus found. The rationale that motivates the choice between equation (1) and equation (3) will be discussed in the following of this appendix. Notice that at each iteration the estimate of the monochromatic and bolometric fluxes also improve because of the improved effective temperature used to interpolate over the grid of model atmosphere. The quantity $R_{\rm obs}$ thus is not exactly constant, but it depends – quite weakly, indeed – on the improved estimate of the effective temperature obtained at each step.

To interpolate over the grid of model atmospheres, both $T_{\rm eff,\it n}$ and [M/H] are needed. This is only possible for our 118 M dwarfs with metallicities obtained from the Bonfils et al. (2005) calibration (Section 2.3). For the remaining stars [M/H] is estimated with the technique presented in Section 4.3.

The behaviour of $R_{\rm theo}$ in different bands for various metallicities and effective temperatures is shown in Fig. 4. In the IR, $R_{\rm theo}$ increases monotonically with increasing $T_{\rm eff}$ above ∼4000 K. If $R_{\rm obs}$ is greater (smaller) than $R_{\rm theo}$, at each iteration $T_{\rm eff,\it n}$ increases (decreases) until it converges to its limiting value. In fact, let us consider the following case:

$$R_{\rm obs} > R_{\rm theo} \tag{A1}$$

which implies

$$\frac{\mathcal{F}_{\rm Bol}({\rm Earth})_{(n-1)}}{\mathcal{F}_{\lambda}({\rm Earth})_{(n-1)}} > \frac{\sigma T^4_{\rm eff,\it n-1}}{\mathcal{F}_{\lambda}({\rm model})_{(n-1)}} \tag{A2}$$

and rearranging to highlight the result

$$T_{\rm eff,\it n} = \left[\frac{\mathcal{F}_{\lambda}({\rm model})_{(n-1)}\mathcal{F}_{\rm Bol}({\rm Earth})_{(n-1)}}{\sigma\mathcal{F}_{\lambda}({\rm Earth})_{(n-1)}}\right]^{1/4} > T_{\rm eff,\it n-1}. \tag{A3}$$

The case $R_{\rm obs} < R_{\rm theo}$ can be similarly proven to give $T_{\rm eff,\it n} < T_{\rm eff,\it n-1}$.

The technique thus converges quickly above $T_{\rm eff}$ about 4000 K, even with quite poor initial estimates of the effective temperature, as it can be more readily understood by looking at the sketch of Fig. A1. Going to cooler effective temperatures, a given $R_{\rm obs}$ intersects $R_{\rm theo}$ twice, i.e. there are two possible iterative solutions. In the case of a very cool star (say below 3500 K in the example of Fig. A1), if $R_{\rm obs}$ is greater than $R_{\rm theo}$, at each iteration $T_{\rm eff,\it n}$ always increases to the solution with highest effective temperature. Similarly, if $R_{\rm obs}$ is smaller than $R_{\rm theo}$ then at each iteration $T_{\rm eff,\it n}$ continues decreasing without reaching a solution. Thus, equation (1) cannot be used for the cooler stars since it only finds one temperature (the hotter one) or none at all. An alternative approach to overcome this limitation would be to sample the entire $R_{\rm theo}$ space, find the two effective temperatures that minimize $|R_{\rm theo} - R_{\rm obs}|$ and choose the proper solution. Other then being more computationally demanding, at cool temperatures the two minima are quite shallow in the IR since $R_{\rm theo}$ inverses smoothly and it might not be obvious which one of the two solutions must be chosen. On the contrary, the use of the flux products when $R_{\rm theo}$ increases with decreasing $T_{\rm eff}$ allows to converge at cool temperatures via equation (3).

It is clear that in any given band, when $R_{\rm theo}$ increases with increasing effective temperature equation (1) must be used, whereas when $R_{\rm theo}$ increases with decreasing effective temperature equation (3) must be used. Only when $R_{\rm theo}$ inverts any dependence on the effective temperature is lost. Fortunately, using multiband photometry, at any given $T_{\rm eff}$ is always possible to find one or more bands for which $R_{\rm theo}$ has a well defined behaviour, i.e. is either monotonically increasing or decreasing, discarding bands for which the dependence is practically flat.

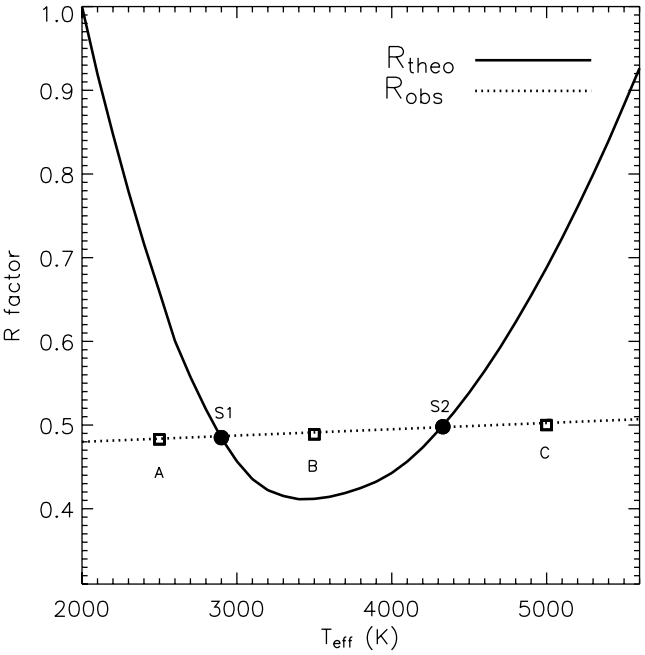

Figure A1. Schematic representation of the degeneracy in the temperature solution in a given band using the IRFM for cool stars. Arbitrary units are used on the *y*-axis. At low temperature, $R_{\rm obs}$ intersects $R_{\rm theo}$ twice, producing two solutions: S1 and S2 (filled circles). If the IRFM starts from A, then $R_{\rm obs} < R_{\rm theo}$ and at each step the new temperature estimate decreases, and diverges away from the desired solution, S1. In case B, $R_{\rm obs} > R_{\rm theo}$ and at each step the new temperature estimate increases until it reaches the hotter solution S2 and terminates. In neither case is the cooler solution S1 found. In case C, $R_{\rm obs} < R_{\rm theo}$ and the IRFM also converges onto solution S2. The use of equation (1) in the IRFM thus finds only the hotter of two temperature solutions and cannot be used for very cool stars. A technique which finds the appropriate solution over many bands has been developed in this paper, and the technical details are discussed here.

Above 4000 K we use equation (1) to estimate $T_{\rm eff,\it n}$ from $J, H, K_{\rm S}$ photometry identically to Casagrande et al. (2006). Note that the choice between equation (1) and equation (3) is important to correctly converge to $T_{\rm eff,\it n}$. However, when the final solution is found, equation (1) or equation (3) returns effective temperatures that agree within ∼5 K in any given band. For this reason, once a solution is found it is possible to have an estimate of the effective temperature from all the other ξ bands (T_{ξ}). The use of both optical and IR colours is crucial for estimating the metallicities, as we explain in Section 4.3. In the optical we estimate T_{ξ} from $V, R_{\rm C}, I_{\rm C}$ photometry; we did not use the *U* and *B* bands since these colours are not available for all the stars and their theoretical modelling is also more uncertain.

For $2500 < T_{\rm eff} < 4000$ K we use equation (1) to estimate $T_{\rm eff,\it n}$ from *J* band and equation (3) to estimate $T_{\rm eff,\it n}$ from *V* and $R_{\rm C}$ band. Below 2500 K we also use equation (3) to estimate $T_{\rm eff,\it n}$ from $I_{\rm C}$. We then average the results obtained in these bands for the next iteration. Again, when a solution is found we compute the effective temperatures T_{ξ} predicted by all the colours (with the exception of *U* and *B* bands, as we already said). For the most metal-poor stars, $I_{\rm C}$ and *J* bands flatten out at very cool temperatures. As suggested by Fig. 4 we have also implemented a more refined approach to ensure that we always use as many bands as possible for which $R_{\rm theo}$ is expected to monotonically increase or decrease. Our code, written in IDL, is available upon request.

© 2008 The Authors. Journal compilation © 2008 RAS, MNRAS **389,** 585–607

Downloaded from http://mnras.oxfordjournals.org/ by guest on January 20, 2015

It is important to note that our technique assigns equal weight to each of the bands used for converging to an effective temperature. It might plausibly be improved by identifying the bands which are more sensitive to effective temperature and those to metallicity in determining these parameters. In this sense, the IRFM can be regarded as a more elegant technique to determine $T_{\rm eff}$, since it works in the Rayleigh–Jeans part of a spectrum and is not much affected by the metallicity. However, below ∼4000 K practically all bands start to show considerable dependence on the metallicity, the only exception being *J* band (Fig. 4). The IRFM is not quite metallicity independent in any case, since the reconstruction of the bolometric flux from multiband photometry still depends on the metallicity used to interpolate in the grid of model atmospheres. We have looked at two scenarios in which MOITE may need to perform, such as only IR or optical photometry being available.

First, we have checked whether any major difference arises by using only *J* band to determine effective temperatures. The behaviour of the flux ratio in such band is in fact expected to be quite unique, with very little metallicity dependence and always increasing as function of $T_{\rm eff}$ (Fig. 4). We did not find any considerable improvement, but only a mean temperature difference of 48 ± 57 K, which we think it stems from the zero-point uncertainties in the *J* band absolute calibration (uncertainty which instead average out using many bands). In addition, relying on one band means the technique is much more exposed to the quality of the photometry in that band.

Secondly, we have studied how the convergence in $T_{\rm eff}$ is affected using only $BVR_{\rm C}$ colours. According to Fig. 4 in the temperature range expected for our stars, it should be possible to use optical colours only. We regard the metallicity as a fixed known parameter and we compute the temperature difference with respect to $T_{\rm eff}$ obtained using both optical and IR colours. We have tested also the difference when IR colours are still used to recover the bolometric flux but not for converging in $T_{\rm eff}$ and when the IR colours are not used at all. Summarizing, the mean difference is of order 15 ± 35 K. This result is very reassuring and also makes the technique promising to be used for M dwarfs for which only optical colours are available.

Therefore, at present, the use of all or only of some optical and IR bands seems to return reliable and consistent results. We plan to further test our findings in forthcoming studies by addressing specifically the sensitivity of different spectral bands to effective temperature and metallicity and eventually refine the technique presented here.

APPENDIX B: THE VEGA AND SIRIUS ABSOLUTE CALIBRATION

In this work we have updated the absolute calibration of Vega in the optical by adopting the new reference spectra of Bohlin (2007) rather than that of Bohlin & Gilliland (2004) and which is expected to be accurate within ∼1 per cent in the range 3200–10 000 Å. In the IR the absolute calibration of Vega is kept the same as in Casagrande et al. (2006), which is based on Cohen, Wheaton & Megeath (2003). In terms of zero-points, the updated fluxes of Bohlin (2007) corresponds to changes of few millimagnitude and affect the derived $T_{\rm eff}$ by 10 K, thus confirming the results obtained in Casagrande et al. (2006).

For some of our stars, we have also *U* photometry (Section 2.1). For Vega we adopt $U = 0.02$ and the same magnitudes as in Casagrande et al. (2006) for the other bands [i.e. $BV(RI)_{\rm C}JHK_{\rm S}$]. *U* filters has proven rather difficult to standardize (e.g. Bessell 1986, 1990b) and adjustment of the *U* zero-points for different temperature ranges has also been discussed (Bessell et al. 1998). *U*, $U - B$ and $B - V$ colours are computed according to the prescription in Bessell (1990b).

The Vega zero-points and absolute calibration thus seem now firmly established in the optical (Bohlin & Gilliland 2004; Bohlin 2007), but some uncertainties (that however do not exceed few per cents) still remain in the IR due to its pole-on and rapidly rotating nature. The IRFM and MOITE temperature scales are intimately related to the adopted IR zero-points and absolute calibration. The possibility of basing our technique on a different photometric system and standard star is a valuable sanity check to the proposed temperature scale.

The SAAO *JHK* photometric system was established by Glass (1974) and its accuracy and zero-points refined and improved over the years by Carter (1990) and Carter & Meadows (1995). Since Vega is unobservable in the Southern hemisphere, the zero-points of the SAAO *JHK* photometric system are based on 25 main-sequence stars ranging from spectral type B1 to A7 (Carter 1990). Sirius is often chosen as a complementary or alternative standard to Vega (e.g. Cohen et al. 1992). Its observed magnitudes and colours in the SAAO *JHK* photometric system are given in Table B1.

Since no absolute flux measurements are available for Sirius, Cohen et al. (1992) decided to absolutely calibrate a Kurucz (1991) Sirius model with respect to Vega, by using observed magnitude difference between Vega and Sirius in different near- and mid-IR bands. Their resulting angular diameter for Sirius was $\theta = 6.04$ mas, 0.9σ larger than the direct measurement (corrected for limb darkening) $\theta = 5.89 \pm 0.16$ mas by Hanbury Brown, Davis & Allen (1974). Recently, new interferometric measurements have become available for Sirius. Davis & Tango (1986) obtained $\theta = 5.93 \pm 0.08$ (when updated limb-darkening coefficients are used; see Kervella et al. 2003), while Mozurkewich et al. (2003) found $\theta = 5.993 \pm 0.108$. All these direct measurements, however, were obtained at optical wavelength, where the limb-darkening corrections are larger and more difficult to assess. Recently, Kervella et al. (2003) have observed Sirius in the near-IR, where the limb-darkening corrections are much smaller, obtaining $\theta = 6.039 \pm 0.019$ mas, in superb agreement with spectrophotometric value of Cohen et al. (1992).

We absolutely calibrate Sirius by scaling its latest Kurucz (2003) synthetic spectrum with the angular diameter measurement of Kervella et al. (2003) and therefore independently of any consideration about Vega. The corresponding effective wavelength and absolute calibration in the SAAO *JHK* filters are reported in Table B2. The error in the angular diameter given by Kervella et al. (2003) implies an uncertainty of only 0.6 per cent in monochromatic absolute fluxes. We adopt a more conservative approach, by taking the standard deviation from all the aforementioned interferometric measurements: these give an uncertainty of 0.066 mas that translates into an uncertainty of circa 2 per cent in fluxes, in good agreement with the global uncertainty of 1.46 per cent estimated by Cohen et al. (1992). Furthermore, the fact the dominant H opacity in A stars is expected to be well understood gives confidence on the adoption of a synthetic spectrum.

We have run the MOITE for stars with SAAO *JHK* photometry (Section 2.2), adopting the zero-points and absolute calibration of Vega in $UBV(RI)_{\rm C}$ and of Sirius in *JHK* (Tables B1 and B2). The

Table B1. Observed magnitudes for Sirius in the SAAO *JHK* system.

J	*H*	*K*	Ref.
−1.387	−1.378	−1.369	Bessell et al. (1998)

Downloaded from http://mnras.oxfordjournals.org/ by guest on January 20, 2015

Table B2. Absolute calibration and effective wavelength of the ground-based SAAO *JHK* photometry of Sirius. Quantities tabulated correspond to the definition of the zero magnitude in each filter.

Band	$\lambda_{\rm eff}$ (Å)	Monochromatic absolute flux (erg cm^{-2} s^{-1} Å^{-1})	Uncertainty (erg cm^{-2} s^{-1} Å^{-1})
J	12 044	1.176e-09	2.570e-11
H	16 282	4.079e-10	8.916e-12
K	22 004	1.367e-10	2.988e-12

The Kurucz model adopted for Sirius has $T_{\rm eff} = 9850$ K, log $(g) = 4.3$, [M/H] $= +0.4$ and microturbolent velocity $\xi = 0\,{\rm km\,s^{-1}}$. The same formalism adopted in Casagrande et al. (2006) is used. Notice that the SAAO *JHK* photometer is equipped with a InSb detector and therefore in generating fluxes from model atmosphere energy integration is the most appropriate.

difference with respect to the use of the 2MASS $JHK_{\rm S}$ photometry and absolute calibration (Cohen et al. 2003) is negligible, thus confirming the adequacy of the absolute calibration adopted in this work and in Casagrande et al. (2006). The mean difference in $T_{\rm eff}$ is 9 ± 3 K ($\sigma = 25$ K), and in both bolometric luminosity and angular diameters is well below 1 per cent. The results provided by the adoption of the absolute calibration of Vega or Sirius are therefore identical within the errors.

SUPPORTING INFORMATION

Additional Supporting Information can be found in the online version of this article.

Table 1. Observable and physical quantities for our sample stars.

Please note: Blackwell Publishing is not responsible for the content or functionality of any supporting information supplied by the authors. Any queries (other than missing material) should be directed to the corresponding author for the article.

This paper has been typeset from a TEX/LATEX file prepared by the author.

Downloaded from http://mnras.oxfordjournals.org/ by guest on January 20, 2015